UNITED STATES

DEPARTMENT OF THE INTERIOR

U.S. GEOLOGICAL SURVEY

[Report - Open file series]

INTERAGENCY REPORT USGS-214

ANALYSIS OF MULTISPECTRAL DATA OF THE SANTA BARBARA OIL SLICK

Final Report

by

S. Stewart
R. Spellicy
F. Polcyn

October 1970

Prepared by the Willow Run Laboratories, Infrared and Optics Laboratory, Institute of Science and Technology, The University of Michigan for the U.S. Geological Survey, Department of the Interior, Contract No. USGS 14-08-0001-12082.

3340-4-F

ANALYSIS OF MULTISPECTRAL DATA OF THE SANTA BARBARA OIL SLICK

Final Report

S. STEWART
R. SPELLICY
F. POLCYN

October 1970

Infrared and Optics Laboratory
Willow Run Laboratories
INSTITUTE OF SCIENCE AND TECHNOLOGY
THE UNIVERSITY OF MICHIGAN
Ann Arbor, Michigan

NOTICES

Sponsorship. The work reported herein was conducted by the Willow Run Laboratories of the Institute of Science and Technology for the U. S. Geological Survey, Department of the Interior, Contract No. USGS 14-08-0001-12082. Contracts and grants to The University of Michigan for the support of sponsored research are administered through the Office of the Vice-President for Research.

Distribution. Initial distribution is indicated at the end of this document.

Final Disposition. After this document has served its purpose, it may be destroyed. Please do not return it to the Willow Run Laboratories.

FOREWORD

This report is one of a series in a program to develop new remote-sensing techniques and to demonstrate their feasibility in a variety of earth-resources applications. The general goal of the University's program is to develop methods of improving and extending current airborne and spaceborne survey capabilities; improvements are sought in the kinds and quality of data obtainable and in the practical application of these data. The program was initiated and is being guided by Marvin R. Holter, Head of the Infrared and Optics Laboratory of the Willow Run Laboratories, a unit of The University of Michigan's Institute of Science and Technology. A list of related reports in this program appears on the following pages.

The work reported in this final report was performed for the U. S. Geological Survey, Department of the Interior, under Contract USGS 14-08-0001-12082. The Willow Run Laboratories' number for this report is 3340-4-F. Advantage was taken of significant laboratory measurement techniques and mathematical models developed under U. S. Coast Guard Contract DOT-CG-92580-A. The period of research extended from 29 September 1969 through 31 March 1970. The Principal Investigator of this research effort was Fabian C. Polcyn, Head of the Interpretation and Information Section of the Infrared and Optics Laboratory. Technical liaison for this project was provided by Mr. John E. Johnston, Department of Interior.

The authors wish to express their appreciation to B. Lastinger, R. Will, and C. Binert for their assistance in the preparation of this report. A preliminary report on the Santa Barbara oil spill was published under the title "Multispectral Sensing of Oil Pollution" by Lowe and Hasell in the Proceedings of the Sixth International Symposium on Remote Sensing of Environment.

RELATED REPORTS

TARGET SIGNATURE STUDY, INTERIM REPORT, VOLUME I: SURVEY (U), R. R. Legault and T. Limperis, Report No. 5698-22-T(I), Institute of Science and Technology, The University of Michigan, Ann Arbor, October 1964, AD 354 166 (CONFIDENTIAL).

TARGET SIGNATURE STUDY, INTERIM REPORT, VOLUME II: RECOMMENDATIONS (U), R. R. Legault and T. Limperis, Report No. 5698-22-T(II), Institute of Science and Technology, The University of Michigan, Ann Arbor, October 1964 (CONFIDENTIAL).

TARGET SIGNATURE STUDY, INTERIM REPORT, VOLUME III: POLARIZATION (U), R. R. Legault and T. Limperis, Report No. 5698-22-T(III), Institute of Science and Technology, The University of Michigan, Ann Arbor, October 1964, AD 354 025 (CONFIDENTIAL).

TARGET SIGNATURE STUDY, INTERIM REPORT, VOLUME IV: BIBLIOGRAPHY (ACOUSTIC, ULTRAVIOLET, VISIBLE, INFRARED, AND RADAR) (U), T. Limperis and R. S. Gould, Report No. 5698-22-T(IV), Institute of Science and Technology, The University of Michigan, Ann Arbor, October 1964, AD 354 232 (SECRET).

TARGET SIGNATURE STUDY, INTERIM REPORT, VOLUME V: CATALOG OF SPECTRAL REFLECTANCE DATA, R. R. Legault, R. S. Gould, and T. Limperis, Report No. 5698-22-T(V), Institute of Science and Technology, The University of Michigan, Ann Arbor, October 1964. (Published as a part of Data Compilation, AD 489 968, see p. vi).

THE INVESTIGATION OF A METHOD FOR REMOTE DETECTION AND ANALYSIS OF LIFE ON A PLANET, M. R. Holter, D. S. Lowe, and J. R. Shay, Report No. 6590-1-P, Institute of Science and Technology, The University of Michigan, Ann Arbor, November 1964.

COMPARATIVE MULTISPECTRAL SENSING (U), M. R. Holter and F. C. Polcyn, Report No. 2900-484-R, Willow Run Laboratories of the Institute of Science and Technology, The University of Michigan, Ann Arbor, June 1965, AD 362 283 (CONFIDENTIAL).

DIURNAL AND SEASONAL VARIATIONS IN RADIATION OF OBJECTS AND BACKGROUNDS, 4.5-5.5 μ SPECTRAL REGION (U), L. D. Miller and R. Horvath, Report No. 6400-32-T, Willow Run Laboratories of the Institute of Science and Technology, The University of Michigan, Ann Arbor, June 1965, AD 362 620 (CONFIDENTIAL).

SPECTRUM MATCHING (U), R. E. Hamilton, Report No. 6400-18-T, Willow Run Laboratories of the Institute of Science and Technology, The University of Michigan, Ann Arbor, June 1965, AD 363 001 (CONFIDENTIAL).

THE INVESTIGATION OF A METHOD FOR REMOTE DETECTION OF LIFE ON A PLANET, L. D. Miller, Report No. 6590-4-F, Willow Run Laboratories of the Institute of Science and Technology, The University of Michigan, Ann Arbor, November 1965.

A COMPREHENSIVE TARGET-SIGNATURE MEASUREMENT PROGRAM, FIRST INTERIM TECHNICAL REPORT, VOLUME I: TECHNICAL DISCUSSION (U), Report No. 7251-3-P(I), Willow Run Laboratories of the Institute of Science and Technology, The University of Michigan, Ann Arbor, December 1965 (CONFIDENTIAL).

UNUSUAL RECONNAISSANCE CONCEPTS INTERIM REPORT, VOLUME I: COUNTERINSURGENCY RECONNAISSANCE AND TARGET SIGNATURE STUDY PROGRAM (U), R. R. Legault and T. Limperis, Report No. 5698-33-P(I), AFAL-TR-65-331, Willow Run Laboratories of the Institute of Science and Technology, The University of Michigan, Ann Arbor, January 1966, AD 370 833 (SECRET).

UNUSUAL RECONNAISSANCE CONCEPTS INTERIM REPORT, VOLUME II: SOURCES OF EXPERIMENTAL ERRORS IN SPECTROPHOTOMETRIC MEASUREMENTS, D. Goerge and T. Limperis, Report No. 5698-33-P(II), AFAL-TR-65-331, Willow Run Laboratories of the Institute of Science and Technology, The University of Michigan, Ann Arbor, January 1966, AD 481 796.

UNUSUAL RECONNAISSANCE CONCEPTS INTERIM REPORT, VOLUME III: A BIBLIOGRAPHY OF RECENT CONTRIBUTIONS ON ELECTROMAGNETIC AND ACOUSTIC SCATTERING, J. Ulrich, Report No. 5698-33-P(III), AFAL-TR-65-331, Willow Run Laboratories of the Institute of Science and Technology, The University of Michigan, Ann Arbor, January 1966, AD 481 817.

UNUSUAL RECONNAISSANCE CONCEPTS INTERIM REPORT, VOLUME IV: A SURVEY OF TARGET SIGNATURE STUDIES (U), D. Goerge and T. Limperis, Report No. 5698-33-P(IV), AFAL-TR-65-331, Willow Run Laboratories of the Institute of Science and Technology, The University of Michigan, Ann Arbor, January 1966, AD 370 850 (SECRET).

UNUSUAL RECONNAISSANCE CONCEPTS: FINAL REPORT (U), R. R. Legault, Report No. 5698-43-F, AFAL-TR-65-345, Willow Run Laboratories of the Institute of Science and Technology, The University of Michigan, Ann Arbor, February 1966, AD 369 331 (SECRET).

A COMPREHENSIVE TARGET-SIGNATURE MEASUREMENT PROGRAM, THIRD INTERIM TECHNICAL REPORT (U), T. Limperis, Report No. 7251-15-P, Willow Run Laboratories of the Institute of Science and Technology, The University of Michigan, Ann Arbor, February 1966 (CONFIDENTIAL).

A COMPREHENSIVE TARGET-SIGNATURE MEASUREMENT PROGRAM, SECOND INTERIM TECHNICAL REPORT, VOLUME I: DATA PROCESSING, STORAGE, AND ANALYSIS (U), Report No. 7251-9-P(I), Willow Run Laboratories of the Institute of Science and Technology, The University of Michigan, Ann Arbor, June 1966 (CONFIDENTIAL).

A COMPREHENSIVE TARGET-SIGNATURE MEASUREMENT PROGRAM, SECOND INTERIM TECHNICAL REPORT, VOLUME II: MEASUREMENT IMPLEMENTATION (U), T. Limperis, Report No. 7251-9-P(II), Willow Run Laboratories of the Institute of Science and Technology, The University of Michigan, Ann Arbor, June 1966 (CONFIDENTIAL).

TARGET SIGNATURE ANALYSIS CENTER: AN ANNOTATED BIBLIOGRAPHY (U), B. Harris, Report No. 7850-1-B, Willow Run Laboratories of the Institute of Science and Technology, The University of Michigan, Ann Arbor, June 1966, AD 373 868 (SECRET).

TARGET SIGNATURE ANALYSIS CENTER: DATA COMPILATION, D. G. Earing and J. A. Smith, Report No. 7850-2-B, Willow Run Laboratories of the Institute of Science and Technology, The University of Michigan, Ann Arbor, July 1966, AD 489 968.

DISPERSIVE MULTISPECTRAL SCANNING: A FEASIBILITY STUDY, FINAL REPORT, J. Braithwaite, Report No. 7610-5-F, Willow Run Laboratories of the Institute of Science and Technology, The University of Michigan, Ann Arbor, September 1966.

AN INVESTIGATIVE STUDY OF A SPECTRUM-MATCHING IMAGING SYSTEM, FINAL REPORT, D. S. Lowe, J. Braithwaite, and V. L. Larrowe, Report No. 8201-1-F, Willow Run Laboratories of the Institute of Science and Technology, The University of Michigan, Ann Arbor, October 1966.

TARGET IMAGE ENHANCEMENT BY MULTISPECTRAL PROCESSING IN REAL TIME (U), R. E. Marshall et al., Proc. IRIS, Vol. XI, No. 1, October 1966 (SECRET).

A COMPREHENSIVE TARGET-SIGNATURE MEASUREMENT PROGRAM, FINAL REPORT (U), T. Limperis, Report No. 7251-21-F, Willow Run Laboratories of the Institute of Science and Technology, The University of Michigan, Ann Arbor, December 1966, AD 378 112 (CONFIDENTIAL).

DATA SIGNATURE ANALYSIS CENTER: DATA COMPILATION (SUPPLEMENT), D. Earing, Report No. 7850-9-B, Willow Run Laboratories of the Institute of Science and Technology, The University of Michigan, Ann Arbor, January 1967, AD 379 650.

TARGET-SIGNATURE MEASUREMENTS, FIRST INTERIM REPORT (U), Report No. 8047-7-P, Willow Run Laboratories of the Institute of Science and Technology, The University of Michigan, Ann Arbor, March 1967, AD 380 008 (CONFIDENTIAL).

OPTICAL SENSING OF MOISTURE CONTENT IN FINE FOREST FUELS, FINAL REPORT, C. E. Olson, Jr., Report No. 8036-1-F, Willow Run Laboratories of the Institute of Science and Technology, The University of Michigan, Ann Arbor, May 1967.

TARGET SIGNATURE ANALYSIS CENTER: DATA COMPILATION (SECOND SUPPLEMENT), D. Earing, Report No. 8492-5-B, Willow Run Laboratories of the Institute of Science and Technology, The University of Michigan, Ann Arbor, July 1967, AD 819 712.

SPECTRAL DISCRIMINATION, VOLUME I: METHODS AND RESULTS OF COMPUTING SPECTRAL RADIANCE STATISTICS FOR REMOTE SENSING IN THE 0.4- TO 1.2-MICRON REGION (U), I. W. Ginsberg and J. L. Beard, Report No. 7850-18-P, Willow Run Laboratories of the Institute of Science and Technology, The University of Michigan, Ann Arbor, July 1967 (CONFIDENTIAL).

TARGET SIGNATURE ANALYSIS CENTER: AN ANNOTATED BIBLIOGRAPHY, SECOND EDITION (U), Report No. 8492-6-B, Willow Run Laboratories of the Institute of Science and Technology, The University of Michigan, Ann Arbor, August 1967, AD 383 572 (SECRET).

SPECTRAL DISCRIMINATION, VOLUME II: ANALYSIS OF SPECTRAL DISCRIMINATION SYSTEMS (U), R. R. Legault, R. E. Hamilton, and J. Penquite, Report No. 8492-9-T, Willow Run Laboratories of the Institute of Science and Technology, The University of Michigan, Ann Arbor, August 1967 (CONFIDENTIAL).

INVESTIGATIONS OF SPECTRUM MATCHING SENSING IN AGRICULTURE (U), F. Polcyn and W. A. Malila, Report No. 6590-7-P, Willow Run Laboratories of the Institute of Science and Technology, The University of Michigan, Ann Arbor, September 1967 (Volume I: UNCLASSIFIED, Volume II: CONFIDENTIAL).

A SIMPLE SPECTRAL DISCRIMINATION TECHNIQUE FOR TARGET RECOGNITION (U), F. J. Thomson, Report No. 6400-118-T, Willow Run Laboratories of the Institute of Science and Technology, The University of Michigan, Ann Arbor, September 1967, AD 384 011 (CONFIDENTIAL).

TARGET SIGNATURE ANALYSIS CENTER: DATA COMPILATION (THIRD SUPPLEMENT) (U), D. Earing, Report No. 8492-12-B, Willow Run Laboratories of the Institute of Science and Technology, The University of Michigan, Ann Arbor, October 1967, AD 384 874 (SECRET).

TARGET SIGNATURE ANALYSIS CENTER: HIGHLIGHTS OF ACTIVITIES (FINAL REPORT) (U), R. R. Legault, Report No. 7850-19-F, AFAL-TR-67-229, Willow Run Laboratories of the Institute of Science and Technology, The University of Michigan, Ann Arbor, November 1967, AD 384 961 (CONFIDENTIAL).

INVESTIGATION OF SPECTRUM MATCHING SENSING IN AGRICULTURE (U), F. C. Polcyn, Report No. 6590-9-F, Willow Run Laboratories of the Institute of Science and Technology, The University of Michigan, Ann Arbor, November 1967 (CONFIDENTIAL).

MULTISPECTRAL DISCRIMINATION OF SMALL TARGETS (U), F. Thomson, Report No. 6400-135-T, Willow Run Laboratories of the Institute of Science and Technology, The University of Michigan, Ann Arbor, December 1967 (CONFIDENTIAL).

TARGET SIGNATURE MEASUREMENTS, SECOND INTERIM REPORT (U), Report No. 8047-18-P, Willow Run Laboratories of the Institute of Science and Technology, The University of Michigan, Ann Arbor, December 1967, AD 385 950 (CONFIDENTIAL).

METALLIC REFLECTION, J. P. Ulrich, Report No. 8492-21-T, Willow Run Laboratories of the Institute of Science and Technology, The University of Michigan, Ann Arbor, March 1968.

TARGET SIGNATURE ANALYSIS CENTER: DATA COMPILATION (FOURTH SUPPLEMENT) (U), D. Earing and E. Haag, Report No. 8492-14-B, Willow Run Laboratories of the Institute of Science and Technology, The University of Michigan, Ann Arbor, July 1968, AD 391 239 (SECRET).

TARGET SIGNATURE ANALYSIS CENTER: HIGHLIGHTS OF ACTIVITIES, 1967, FIRST INTERIM REPORT (U), Report No. 8492-17-P, Willow Run Laboratories of the Institute of Science and Technology, The University of Michigan, Ann Arbor, July 1968 (SECRET).

TARGET SIGNATURE ANALYSIS CENTER: DATA COMPILATION (FIFTH SUPPLEMENT), D. Earing, Report No. 8492-15-B, Willow Run Laboratories of the Institute of Science and Technology, The University of Michigan, Ann Arbor, August 1968.

CALIBRATION OF AN AIRBORNE MULTISPECTRAL OPTICAL SENSOR, L. M. Larsen and P. G. Hasell, Jr., Report No. 6400-137-T, Willow Run Laboratories of the Institute of Science and Technology, The University of Michigan, Ann Arbor, September 1968.

STATISTICAL SPECTRAL ANALYZER AND TARGET RECOGNITION COMPUTER (SPARC), FINAL REPORT (U), F. J. Kriegler and M. M. Spencer, Report No. 8640-17-F, Willow Run Laboratories of the Institute of Science and Technology, The University of Michigan, Ann Arbor, September 1968 (CONFIDENTIAL).

TARGET SIGNATURE MEASUREMENTS, FINAL REPORT (U), Report No. 8047-28-F, Willow Run Laboratories of the Institute of Science and Technology, The University of Michigan, Ann Arbor, September 1968 (CONFIDENTIAL).

TARGET SIGNATURE ANALYSIS CENTER: DATA COMPILATION (SIXTH SUPPLEMENT), D. Earing, Report No. 8492-26-B, Willow Run Laboratories of the Institute of Science and Technology, The University of Michigan, Ann Arbor, October 1968.

ABSTRACT

The potential of multispectral remote sensing to aid in the detection and location of oil slicks is being investigated. Multispectral data were collected on the Santa Barbara Channel oil slick in the region from ultraviolet to thermal infrared at 2000-ft and 10,000-ft altitudes and at three different times of the day. The ultraviolet and blue region offered the most contrast for thin films of oil and dispersant, while the thermal infrared appeared the most promising for detecting thicker globules of oil. Multispectral data gathered for oil thickness determinations were investigated using (1) a theoretical oil-water mathematical model of reflectance, and (2) laboratory measurements of the optical properties of oil samples and dispersant. The contrasts predicted by the model were in general agreement with the imagery, especially in those spectral regions where scattering coefficients were known from measurements. Detection of the slick in the 0.40- to 0.44-μm region at 10,000 ft offers promise for satellite monitoring of oil slicks.

SPECIAL NOTICE

Subsequent to the preparation of this report, the wavelength bands for the multispectral imagery have been found to be in error. The new wavelength designations based upon recent sensor tests are as follows:

Wavelength Designated in This Report	New Wavelength Designations
0.32-0.38 μm	0.32-0.38 μm
0.40-0.44 μm	0.41-0.43 μm
0.44-0.46 μm	0.43-0.455 μm
0.46-0.48 μm	0.455-0.47 μm
0.52-0.55 μm	0.50-0.52 μm
0.58-0.62 μm	0.545-0.58 μm
0.60-0.72 μm	0.63-0.68 μm
0.80-1.0 μm	0.75-0.855 μm

These differences in wavelength designations do not change the conclusions reached in the report.

CONTENTS

FIGURES

TABLES

ANALYSIS OF MULTISPECTRAL DATA OF THE SANTA BARBARA OIL SLICK

Final Report

1
INTRODUCTION AND SUMMARY

The rapidly growing economies of nations have created a world-wide demand for more and cheaper oil. Huge super tankers, capable of carrying more than 30,000 tons of oil, are currently operational on the seas, and still bigger ones are being designed. New off-shore wells are planned to meet the demand. The present world oil production stands near 1.8×10^{15} gal/year [1]. With quantities such as this being produced and shipped across the seas, some spillage is inevitable. Even a leakage rate as small as 0.1%, which has been estimated as a typical loss in transportation, results in vast amounts of oil being spilled into the sea. The problem of oil pollution becomes one of serious concern.

The well-publicized Torrey Canyon and Santa Barbara episodes exemplify the magnitude of the problem. Serious damage to water fowl and aquatic life, as well as extensive damage to beaches, occurred from these accidents despite attempts to contain the oil spills. As more and more advances are made in the technology of containment and dispersing of oil slicks, the major concern becomes one of locating oil slicks at sea so that corrective measures can be taken before serious damage is done.

At the request of Dr. John DeNoyer of the U. S. Department of the Interior, personnel of The University of Michigan mapped the oil pollution in the vicinity of Santa Barbara with its airborne multispectral system. The flight was made under Contract 14-12-517 with the Federal Water Quality Administration. The purpose of the flight was (1) to gain some qualitative insight into the problem of locating oil slicks from the air, and (2) to determine the effects and distribution of the dispersant being sprayed on the oil at the time of the surveys. In addition, kelp beds near shore were mapped to determine the amount of oil impregnation there.

The more significant imagery obtained from these flights over the oil slick and kelp beds is shown in Section 2.2 of this report. The major observation made from this imagery was that the oil slick gave a positive contrast against water in the ultraviolet (UV) and blue spectral regions while showing no contrast in the red and near-infrared (NIR) regions. Thermal data indicated that the thick streamers of oil showed up approximately 2.5°F colder than the surrounding bodies of water. However, aerial photographs revealed that the thick streamers of oil present in the slick did not give the greatest contrast in the UV; instead, what appeared to be a thin oil film gave the strongest return. Observations such as these made it apparent that more than just field measurements were needed if a thorough investigation of the problem of detecting and mapping oil on water was desired. Therefore, a laboratory measurements program was undertaken to measure the optical characteristics of oil and its dispersant. Samples of the Santa Barbara oil slick and dispersant were sent to The University of Michigan by the Federal Water Quality Administration (FWQA) and measurements were made of the index of refraction, and extinction, absorption, and scattering coefficients in the spectral region from 0.32 μm to 6.2 μm. In addition, a theoretical model of the oil-on-water interface was used to predict the observed reflectance off the oil using the oil thickness and the above measured quantities. A detailed discussion of the model and the optical properties measured are included in appendices at the end of the report.

The output from the model which is reported in Section 2.3 indicated that the high UV return resulted from increased scattering action caused by the application of the dispersant to the oil. Thickness determination by means of the model indicated the UV band to be impractical but did show a potential for the NIR or thermal bands. Angle effects were also considered, and Section 2.4 shows that the optimum time for viewing oil slicks using the UV region lay in the early morning and late afternoon.

Imagery obtained at 10,000 ft indicated the slick to be still observable in the blue and thermal regions, although the contrast was lower. Section 2.5 reports some of the imagery obtained at this higher altitude, and also contains an analysis of oil slick mapping from satellite altitudes. This analysis uses selected narrow portions of the planned spectral bands in the NASA ERTS A & B systems and initially indicated that detection of thin oil films would be remote in the spectral channels currently being considered for the ERTS satellite. The measurements and observations indicated in Section 2 provide a well-balanced study into the feasibility of detecting and mapping oil slicks. The final section summarizes these results and recommends that future experiments in the areas of oil slick detection and monitoring for thickness be conducted to verify the validity of the existing model and, also, to extend the model to the thermal region for possible thickness determinations there. In addition, a more detailed analysis (through use of the simulated data from 10,000 ft) of the potential of a satellite monitoring system is suggested.

2
ANALYSIS OF MULTISPECTRAL AIRBORNE IMAGERY

2.1. THE MULTISPECTRAL SCANNER

Before the multispectral imagery is analyzed, one should first be basically familiar with the operation of the scanner. The equipment used to map the Santa Barbara oil slick has been described in much detail in other publications [2], so only a brief description will be given here. The scanner system, which is mounted in a C-47, actually consists of two much modified AN/AAS-5 scanners. The two scanners, both with double-ended optics, have the capability of collecting data in 17 spectral channels. Because of thermal calibration plates mounted in one of the units, the swath angle of the one scanner was reduced from the original design angle of 80^{o} to 38^{o}. For the Santa Barbara mission, this "narrow field" thermal scanner was equipped with a filtered GeHg detector in one end and a 3-element InSb detector in the other. A 12-channel spectrometer, operating in the visible and near-IR regions, filled one end of the other scanner while the detector occupying the remaining end was varied from one flight to the next. These included a UV detector on one of the flights, an 8.0- to 13.5-μm tri-metal detector on another, and a 3-element InSb detector on the third flight. The wavelength capabilities of each detector package are given in Table 1.

TABLE 1. WAVELENGTH CAPABILITIES OF DETECTORS

Filtered UV Photomultiplier	0.32-0.38 μm
12-Channel Spectrometer	12 bands from 0.40 to 1.0 μm
3-Element InAs	1.0-1.4 μm, 1.5-1.8 μm, 2.0-2.6 μm
3-Element InSb	1.0-1.4 μm, 2.0-2.6 μm, 4.5-5.5 μm
Filtered InSb	4.5-5.5 μm
Filtered GeHg	8.0-13.5 μm
Filtered Hg-Cd-Te	8.0-12.5 μm

The actual operation of the scanner is relatively simple. As the aircraft carrying the multispectral scanner moves forward, successive scan lines are recorded (Fig. 1), resulting in a continuous strip of data produced line by line. The data are recorded on magnetic tape and played back at a later date for analysis.

2.2. ANALYSIS OF IMAGERY

At the time of the surveys (6-7 March 1969), the main leakage had been stopped, and the leakage rate was estimated at between 1000 and 2000 gal/day. The major apparent slick was confined to the vicinity of the leaking well on Platform A, and the scattered oil was well broken up. Several flight lines were flown in order to observe not only the extent of the spillage from the platform, but also if oil damage to kelp could be seen on the coastline.

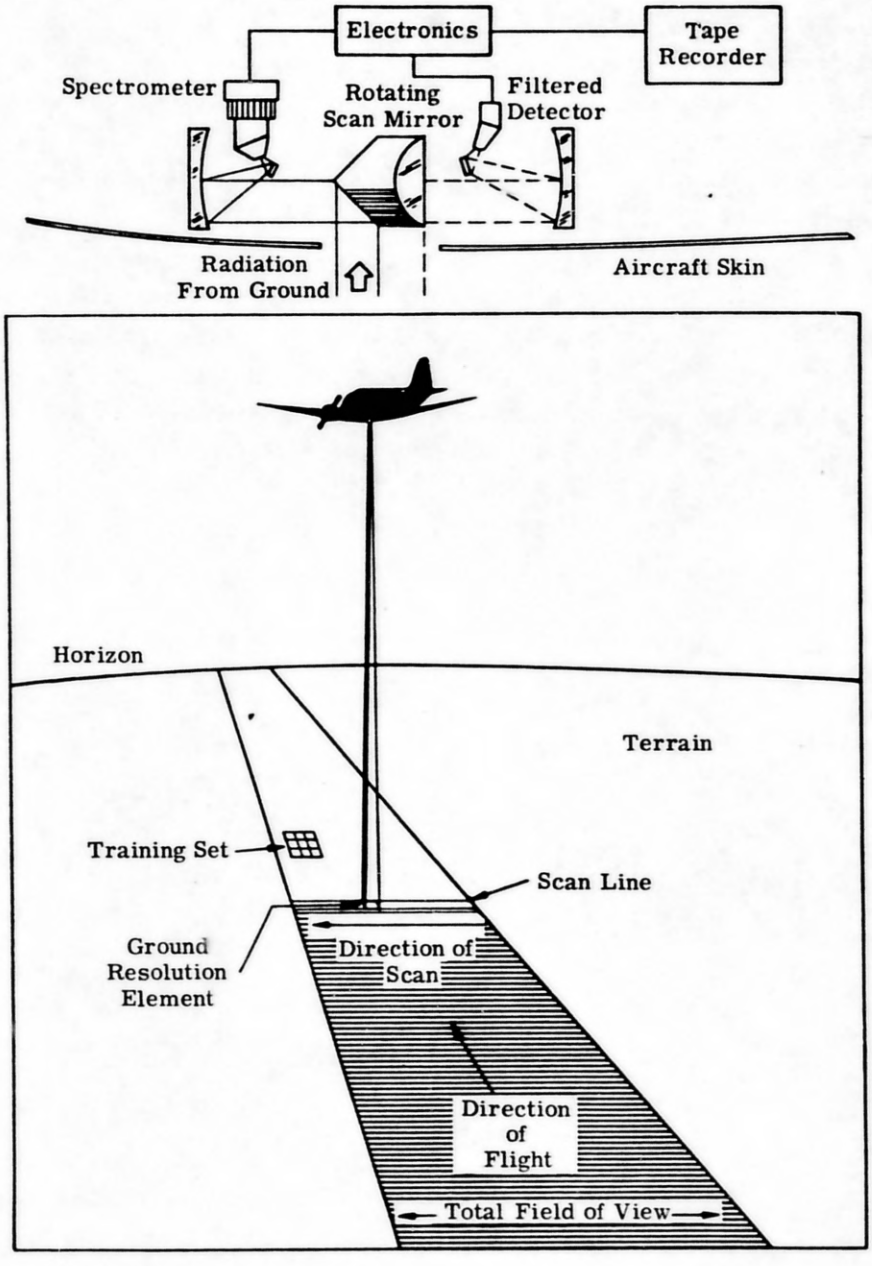

FIGURE 1. MULTISPECTRAL DATA COLLECTION

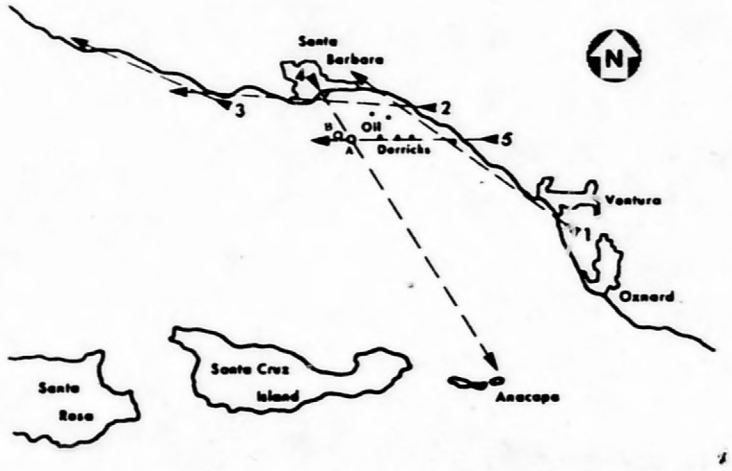

FIGURE 2. MISSION FLIGHT LINES (6-7 MARCH 1969). A and B indicate Union Oil's Platforms A and B.

The flight lines actually flown are shown in Fig. 2. The effects of view and illumination angles and water temperature on the imagery were investigated by choosing three flight times for gathering data: early morning, noon, and afternoon. Table 2 shows the wavelengths used in the scanners during each of these flights. Two altitudes were flown: one at 2000 ft and one at 10,000 ft.

Shown in Fig. 3 is a panchromatic photograph of the leaking Platform A taken at approximately 8:15 a.m. on the early morning flight. The photograph was taken with a K-17 camera at 2000 ft with a K-2 star filter (a haze filter which rejects blue light). The large light area to the right of the platform is foaming dispersant being sprayed onto the oil from a ship. As evident from this figure, the oil slick is not very apparent at this time of day if we use black and white photography. In fact, to the untrained observer, the kelp beds near shore (see Fig. 4) appear more likely to be oil than the oil itself. Fortunately, the signatures (or colors) of oil and kelp are different enough that they can be easily separated using either multispectral imagery or color infrared (IR) photography. Figure 4 shows normal color and color IR photographs of a

TABLE 2. WAVELENGTHS OF SCANNERS AS A FUNCTION OF FLIGHT TIME

Detector	UV P.M.*	Visible P.M.*											InAs			InSb			HgCdTe	Mod Te
Wavelength (μm)	0.32 0.38	0.40 0.44	0.44 0.46	0.46 0.48	0.50 0.52	0.52 0.55	0.55 0.58	0.58 0.62	0.62 0.66	0.66 0.72	0.72 0.80	0.80 1.00	1.0 1.4	1.5 1.8	2.0 2.6	1.0 1.4	2.0 2.6	4.5 5.5	8.0 13.5	8.0 12.5
3:00 p.m. March 6		x		x	x	x	x	x	x	x	x	x	x	x	x	x	x	x	x	
6:15 a.m. March 7	x	x	x	x	x	x	x	x	x	x	x	x				x	x	x	x	
11:30 a.m. March 7		x	x	x	x	x	x	x	x	x	x	x				x	x	x	x	x

*P.M. - Photomultiplier Tube

FIGURE 3. PANCHROMATIC AERIAL FILM OF SANTA BARBARA OIL SLICK. March 7, 1969, 8:15 a.m. Altitude: 2000 ft.

large kelp bed near Santa Barbara. In Fig. 4(a), the dark patches in the water could be mistaken for oil, but the color IR photograph [Fig. 4(b)] clarifies the situation. In color IR, green objects appear as red so that this particular kelp (which uses mainly the pigment chlorophyll for photosynthesis) does show up quite red. Figure 5 shows a photograph of a similar kelp bed obtained from the airborne imagery; here, the spectral character of the kelp is quite pronounced.

Because oil would appear dark in color IR film, the amount of oil impregnated in kelp can be determined by taking simultaneous photographs of kelp beds with either panchromatic or color film and color IR film. The extent of the kelp beds could be determined by the black and white picture, while the non-red areas of kelp in the color IR would indicate oil pollution. Although the camera used to obtain the photographs in Fig. 4(b) was not operating correctly, apparently no noticeable amount of oil was impregnated in these particular kelp beds, since all the kelp appears red. Of course, if the oil happens to impregnate only the edge of the kelp bed, a greater resolution than shown in Fig. 4 from 10,000 ft would be required.

Unfortunately, it is not as easy to distinguish oil from water as it is to distinguish oil from kelp. Figure 6 shows the oil slick in the vicinity of the platform in color and color IR photographs taken at the same time as the black and white photograph in Fig. 3. Although the contrast

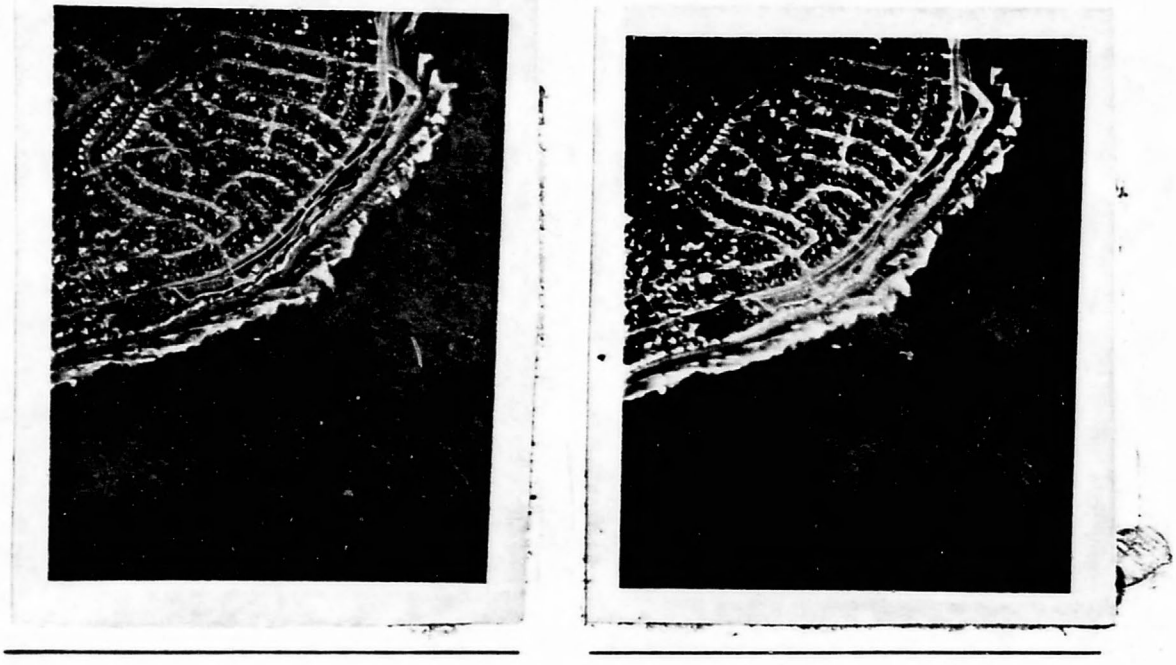

(a) Color (b) Color IR

FIGURE 4. COLOR AND COLOR IR PHOTOGRAPHS OF KELP BEDS. Near Santa Barbara, California, March 7, 1969, 8:15 a.m. Altitude: 10,000 ft.

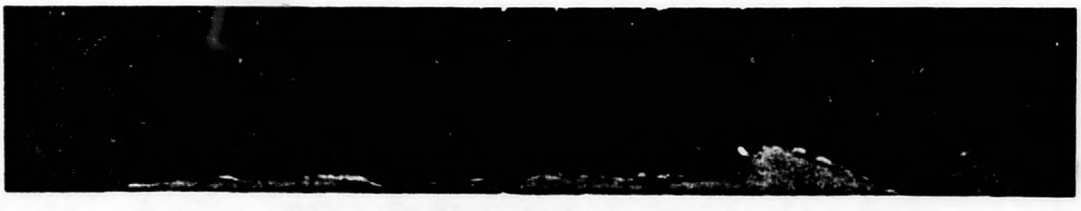

(a) Infrared (0.8-1.0 μm)

(b) Ultraviolet (0.32-0.38 μm)

FIGURE 5. ULTRAVIOLET AND INFRARED IMAGES OF KELP

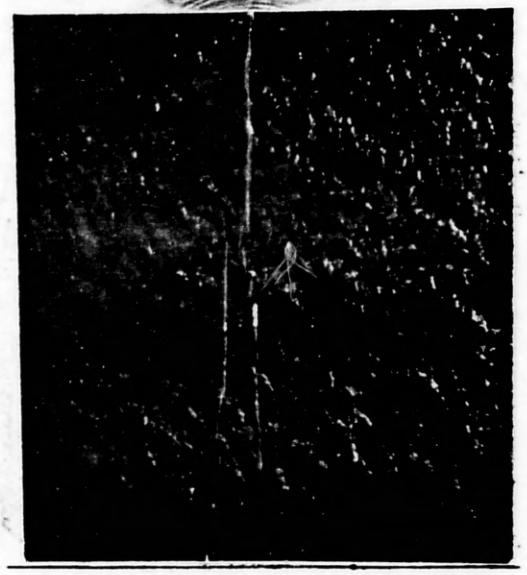

(a) Color

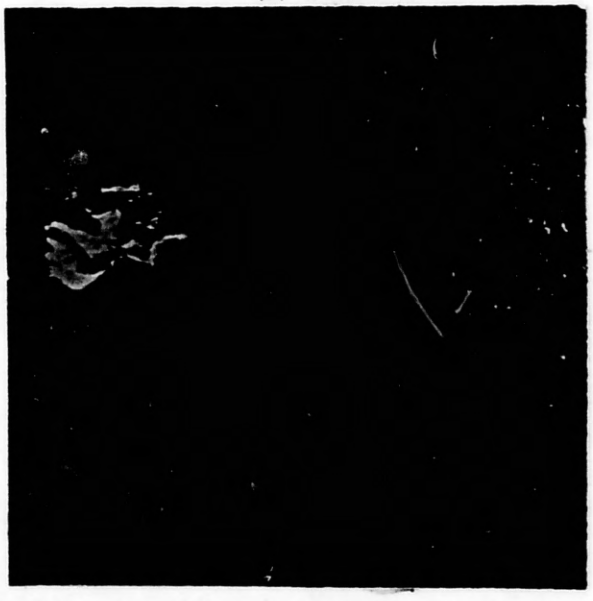

(b) Color IR

FIGURE 6. COLOR AND COLOR IR PHOTOGRAPHS OF MAIN OIL SLICK FROM PLATFORM A. March 7, 1969, 8:15 a.m. Altitude: 2000 ft.

is poor, the blue-black streaks of oil which are visible in the color print are more difficult to distinguish in the color IR. Only when the oil has reduced wave action by decreasing water surface tension can the slick be seen in color IR, and even then, it is only through an increase in specular reflection. Figure 7 shows just such an example. This particular photograph was taken at 11:30 a.m., when the specular return from the sun is quite pronounced. The multispectral imagery, on the other hand, illustrates a pronounced contrast between the oil and the water. Figure 8 shows the oil slick at 8:15 a.m. in 8 bands in the visible and UV wavelengths. The UV band shows the greatest contrast, while at wavelengths longer than 0.54 μm, no contrast is seen. The oil slick in this photograph is about 7 1/2 miles long.

A significantly different pattern is observed in the thermal region (8.0-13.5 μm). Shown in Fig. 9 is a comparison of the UV image with the thermal image. It is obvious that the colder areas (indicated by the dark patches) do not correlate with those areas designated as oil in the UV image. In fact, these colder areas in the thermal image appear darker than the surrounding oil areas in the UV image, although they are still much brighter than the water. Color photographs taken at the same time as those in Fig. 6 indicate the colder areas to be heavy, thick globs of oil that have not been affected as yet by any dispersant. The bright areas in the UV image appear as milky, green substances in this photograph (Fig. 6). Laboratory measurements have shown that the dispersant being sprayed onto the oil foams into a soap-like substance, and it appears that what is being shown as oil in the UV image is actually a thin film mixture of oil and dispersant with the oil suspended beneath the surface of the water. It seems probable that the high UV reflectance observed from the oil-dispersant mixture is caused by (1) the foaming geometry of the oil-dispersant interaction and (2) volume scattering. The thick oil globules, on the other hand, are very smooth and, therefore, do not have as high a UV reflectance as the thin, foaming, oil-dispersant layer. Of course, the high UV return is also caused, in part, by the physical properties of the oil, as will be shown in the next section, so that one would still expect a significant UV return even from the unmixed oil. Examination of Fig. 9 bears this out.

2.3. MODEL PREDICTIONS AND CONCLUSIONS

In order to study in more detail the phenomenon observed in the previous section, samples of the Santa Barbara oil and dispersant were obtained, and the optical properties were measured. The techniques used to obtain the extinction and scattering coefficients and the index of refraction are given in Appendix II along with the data. A reflectance model, developed under Coast Guard Contract No. DOT-CG-92580-A and whose derivation is given in Appendix I, was modified to accept the data obtained for the Santa Barbara samples. Once the necessary optical properties of the oil and dispersant were determined, the model was programmed on our CDC-1604 computer and used to predict from these properties the radiances and contrasts which should be seen by a remote-sensing system. Water, oil, and dispersant were treated for various thick-

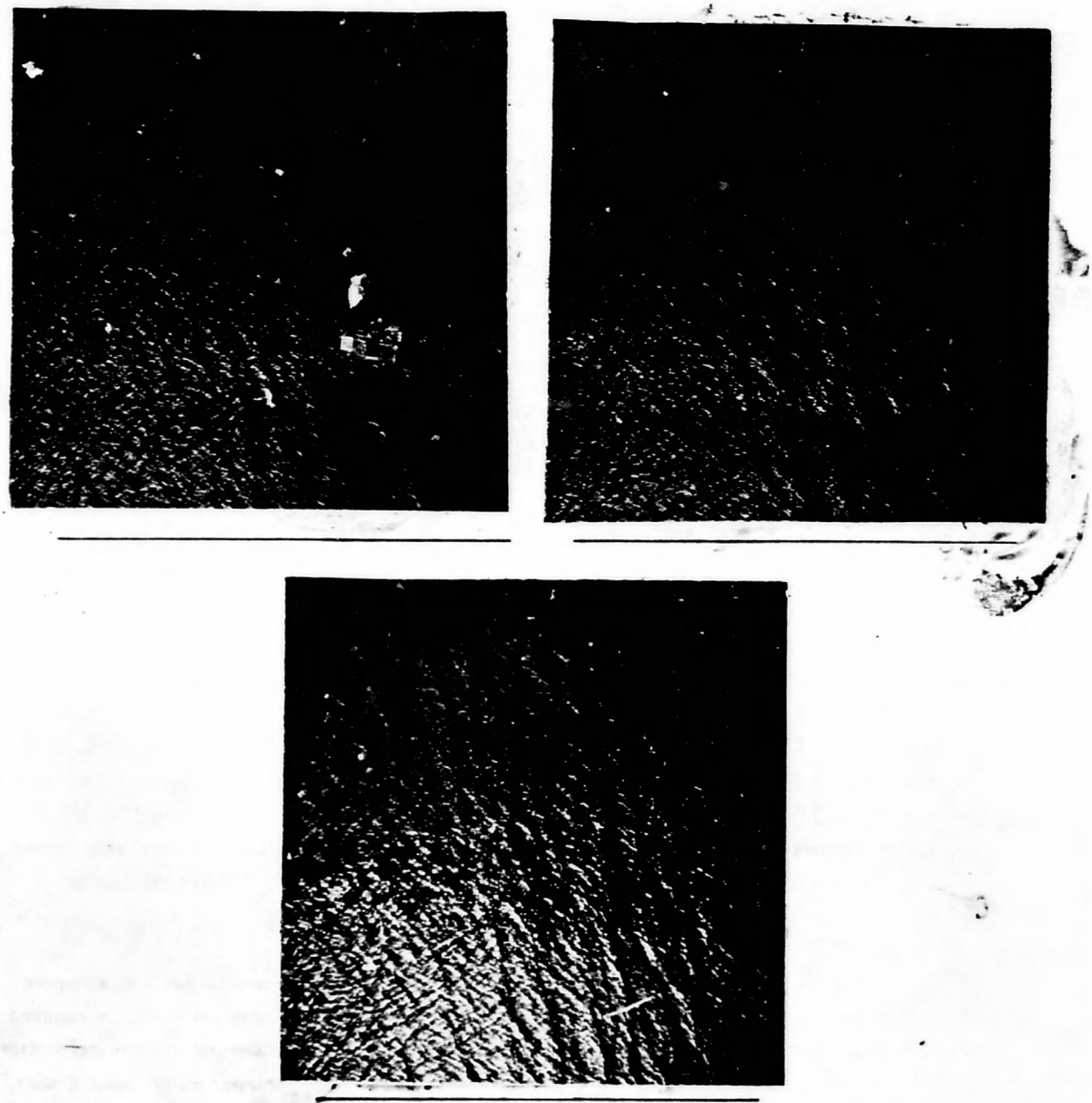

(b) Color IR

FIGURE 7. COLOR AND COLOR IR PHOTOGRAPHS OF OIL SLICK. March 7, 1969, 1:30 p.m. Altitude: 2000 ft.

(a) 0.32-0.38 μm

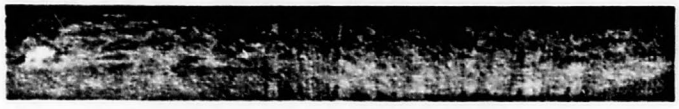

(b) 0.40-0.44 μm

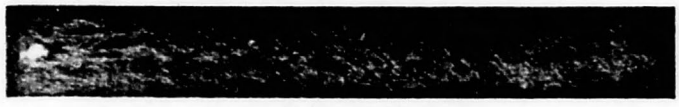

(c) 0.44-0.46 μm

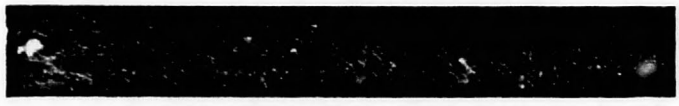

(d) 0.46-0.48 μm

(e) 0.52-0.55 μm

(f) 0.53-0.62 μm

(g) 0.66-0.72 μm

(h) 0.80-1.00 μm

FIGURE 8. MULTISPECTRAL IMAGERY OF OIL SLICK. March 7, 1969, 8:15 a.m. Altitude: 2000 ft.

(a) Ultraviolet (0.32-0.38 μm)

(b) Infrared (8.0-13.5 μm)

FIGURE 9. ULTRAVIOLET AND INFRARED IMAGES OF OIL SLICK. March 7, 1969, 8:15 a.m. Altitude: 2000 ft.

nesses, sun elevations, and observation angles. Figures 10 through 14 present plots of radiance as a function of wavelength for representative cases. Sun angles of 0^o and 50^o and observation angles of 15^o and 60^o were chosen for thicknesses varying from 10^{-2} mm to 0.5 mm. Thicknesses greater than 0.5 mm are not presented because no significant differences appear.

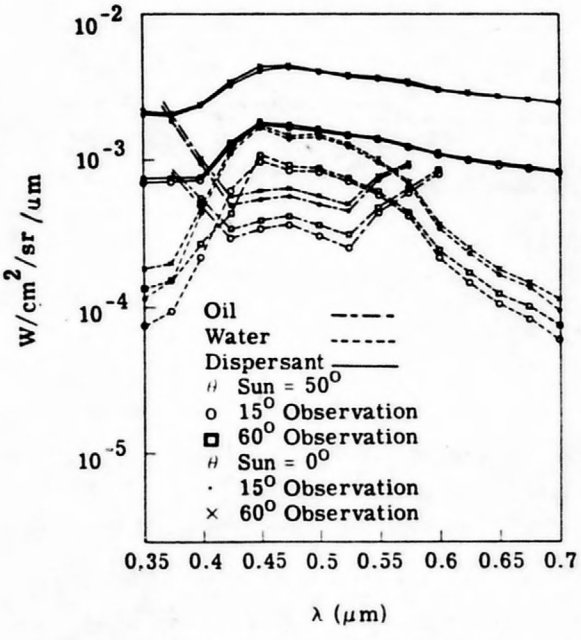

FIGURE 10. OIL AND DISPERSANT RADIANCE (0.5-mm THICKNESS)

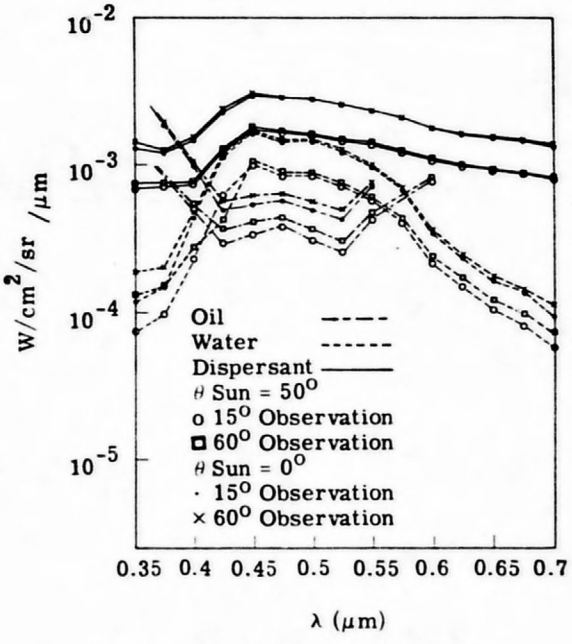

FIGURE 11. OIL AND DISPERSANT RADIANCE (0.25-mm THICKNESS)

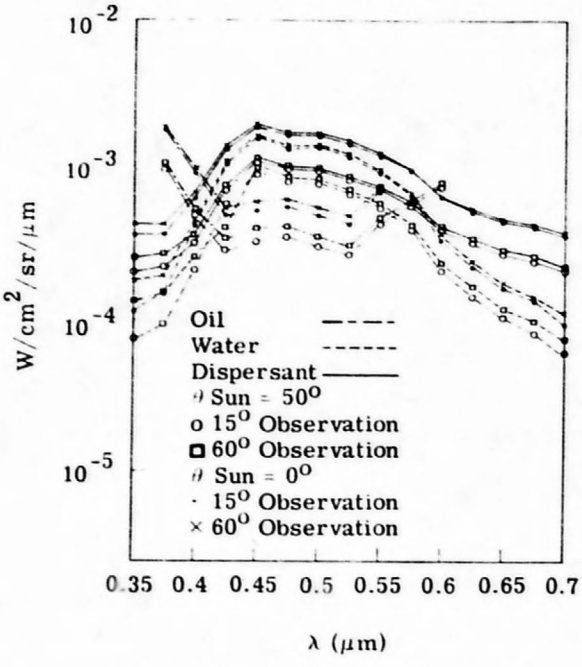

FIGURE 12. OIL AND DISPERSANT RADIANCE (0.05-mm THICKNESS)

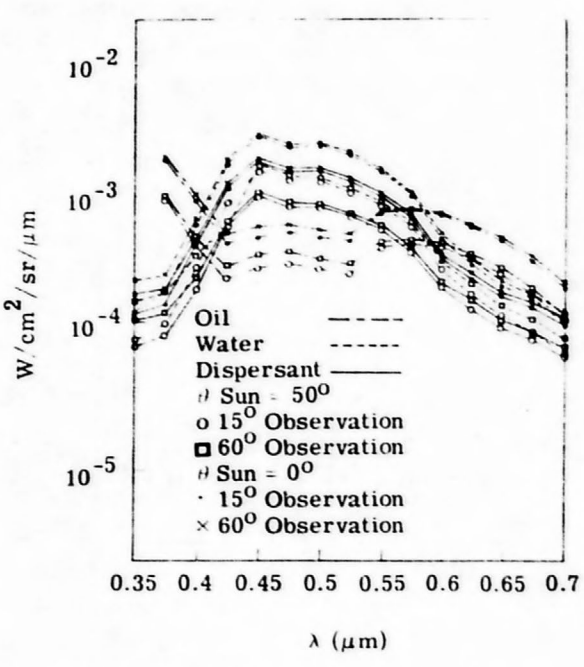

FIGURE 13. OIL AND DISPERSANT RADIANCE (0.01-mm THICKNESS)

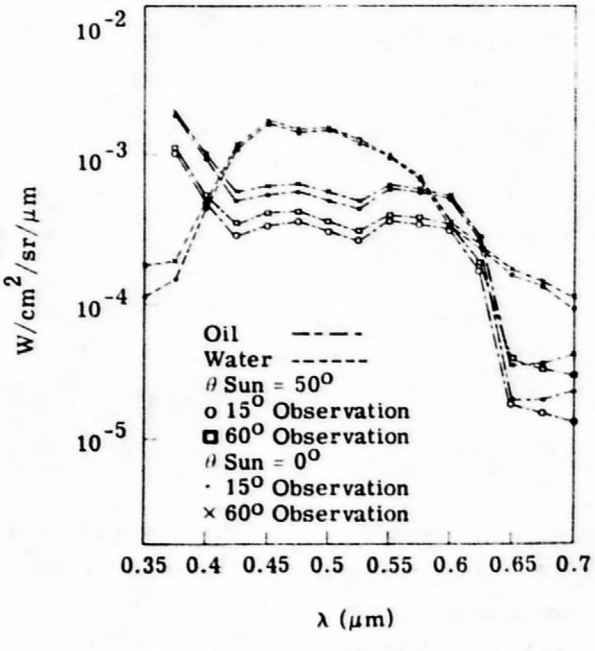

FIGURE 14. OIL AND WATER RADIANCE USING DIFFERENT OIL SCATTERING CO-EFFICIENTS (0.05-m THICKNESS)

For remote-sensing purposes, the significant feature of these plots is the separation of the sample and water curves, since this represents the contrast which will be observed between the sample and sea water. If the sample curve is above the corresponding water curve, a positive contrast is indicated; that is, the sample will appear brighter than the water. If the sample curve lies below the corresponding water curve, a negative contrast is indicated and the sample will appear darker than the water. Therefore, it is obvious that both the oil and dispersant should exhibit positive contrasts below 0.4 μm. As the film thickness is varied, however, the radiance of the oil remains unchanged, while the radiance of the dispersant decreases as the film thickness is decreased. This is because the mechanism producing this contrast, in the case of the oil, is predominantly a front-surface reflection and/or scattering produced in the uppermost regions of the oil layer. For the dispersant, however, the mechanism is more a volumetric scattering within the layer. It is also significant that the oil-water contrast becomes negative between approximately 0.41 μm and 0.55 μm with zero contrast at the extreme upper end of this region.

These characteristics show that the region below 0.4 μm is well suited to the detection of oil or dispersant on water. However, thickness determinations for oil in this region are not feasible since radiance values do not vary with thickness. But for more transparent and more highly scattering substances such as the dispersant, thickness variations are seen throughout the spectrum from 0.35 μm to 0.7 μm, which implies the possibility of a thickness determination for such materials as the dispersant by comparing intensities of various channels.

Since preliminary, qualitative considerations indicated that the scattering coefficient of the Santa Barbara oil was very small beyond 0.6 μm, laboratory data were not obtained beyond this point. It was therefore impossible to make any definite conclusions regarding possible thickness variations beyond 0.6 μm. However, extrapolation of the existing scattering data to 0.7 μm as shown in Figs. 13 and 14 for thicknesses of 0.01 mm and 0.05 mm shows an obvious variation in radiance with thickness and indicates that extension of scattering data beyond 0.6 μm may be fruitful. The fact that variations are seen beyond 0.6 μm, while none are in evidence in the region from 0.35 to 0.6 μm, is attributable to the increase in transmission of the oil in the region beyond 0.6 μm making volumetric effects such as scattering more significant.

Although the model was used to determine radiances from 0.7 μm out to 2.6 μm, these data are not presented here because the lack of scattering data for the oil made it impossible to draw any significant conclusions.

The predicted angular variations are constant with wavelength and thickness as expected. As previously discussed, the fact that the greatest variation is seen in the case of the oil indicates that front surface effects dominate for this material. The contrast variations caused by sun and observation angle can be used to select optimum angles for oil slick detection. However, agreement with scanner data should be verified.

2.4. THERMAL AND ANGLE EFFECTS

As the next step in examining the imagery, a temperature contour was made of the oil slick observed during the 11:30 a.m. flight (Fig. 15). The coldest part of the oil is 2.5°F cooler than the surrounding water and appears to occur in the middle of the oil slick where the oil is thickest. Also, the coldest areas occur near the platform above the point where the oil is seeping up through the ocean floor. This indicates that the crude oil rising to the surface is initially cooler than the surface waters and heats up only after it has been dispersed or has had time to absorb heat from its surroundings. The temperature differences of this particular oil slick have also been studied by other researchers [3]. However, their results were somewhat different from those observed in The University of Michigan survey. Estes and Golomb [3] reported a mottled pattern to their thermal image of the slick showing both hotter and cooler patches of oil. We observed only oil that was cooler than the surface water. Measurements of thermal emissivities made on similar oils at The University of Michigan indicate that oil's emissivity is, in fact, only slightly lower than that of water, so that it is unlikely for the oil and water to be at the same temperature. It is evident that more ground truth, in addition to a working thermal model, is required before the thermal effects are fully understood.

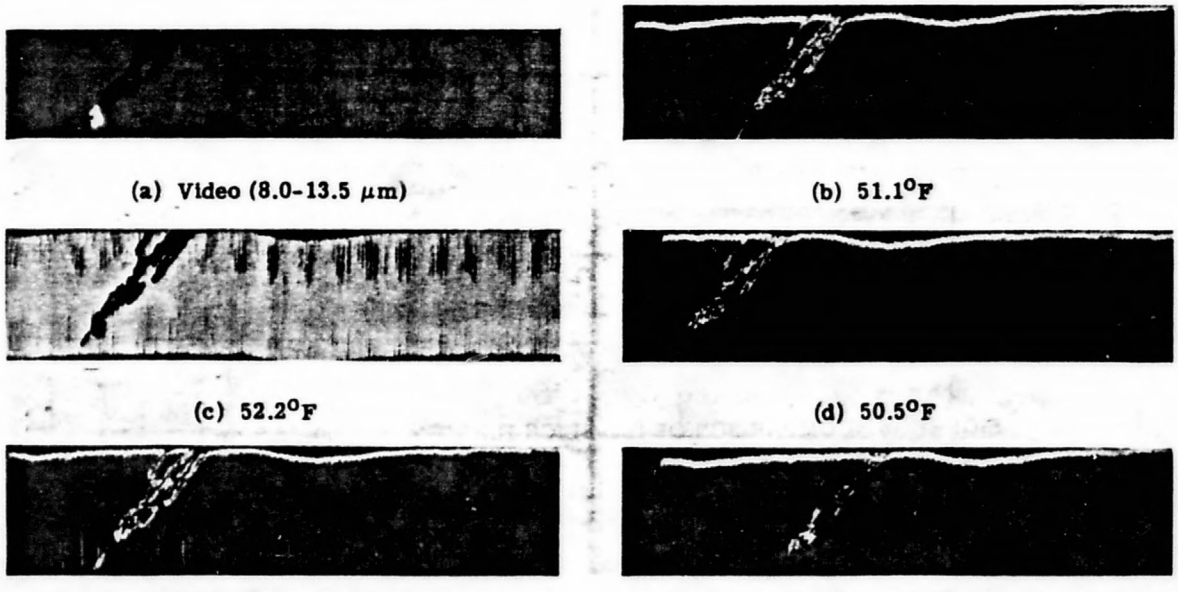

FIGURE 15. THERMAL SLICING OF MAIN OIL SLICK.
March 7, 1969, 1:30 p.m. Altitude: 2000 ft.

is evident that more ground truth, in addition to a working thermal model, is required before the thermal effects are fully understood.

The motion of the slick on a day-to-day basis was also a subject of interest. If Fig. 16a is compared with Fig. 16b, a 45° shift in the direction of the oil slick is observed. The data shown were obtained in the 8.0- to 13.5-μm region along identical flight paths. Table 3 summarizes the meteorological conditions for the three flights. Although accurate meteorological ground data were not readily available, aircraft logs indicated an approximate tail wind for the early morning (6:15 a.m.) flight, while a 40° cross wind prevailed for the noon (11:30 a.m.) flight. Thus, it appears that the oil slick drifts according to wind direction. This is in agreement with the information provided in Ref. [1], which states that oil on a calm sea will be blown about by the wind with a velocity equal to 3% of the wind speed. Figure 17 shows another oil slick from the Santa Barbara oil spill which has drifted near the shoreline close to Santa Barbara. Because of differences in thermal heating, diurnal onshore and offshore breezes result and blow this oil slick about. At 3:00 p.m. (bottom photo), the oil slick is near shore even though the tide is ebbing. By 6:15 a.m. (top photo) the following morning, the slick has moved offshore because of the nightly offshore breeze even though this also is a low tide period. This points out that the oil slick responds more to wind action than tidal currents.

8-13.5 μm

(a) March 7, 1969, 8:15 a.m. Altitude: 2000 ft.

8-13.5 μm

(b) March 7, 1969, 1:30 p.m. Altitude: 2000 ft.

FIGURE 16. COMPARISON OF OIL SLICK DIRECTIONS (8.0-13.5 μm)

From these figures, it is obvious that oil slicks (or, more appropriately, oil-dispersant mixtures) can be located using UV or blue bands. It is important to note, however, that during the noon (11:30 a.m.) flight, this oil slick was not observed (see Fig. 17b) nor was the main oil leakage slick at Platform B. Evidently, the lower the sun elevation, the more apparent the oil slick. Although this is not in agreement with the theory proposed in Section 2.3, the evidence points to this conclusion. The model, however, assumed isotropic scattering, which now appears, perhaps, to be an incorrect assumption.

TABLE 3. METEOROLOGICAL CONDITIONS FOR FLIGHTS

Flight Time	3:00 p.m. 3/6/69	6:15 a.m. 3/7/69	11:30 a.m. 3/7/69
Oil Slick Direction	165°	145°	100°
Plane Heading	145°	145°	145°
Wind Direction (surface)	340°	300°	260°
Wind Velocity	12 knots	20 knots	5 knots
Estimated Oil Slick Drift Velocity	0.36 knots	0.60 knots	0.15 knots

2.5. LOCATING OIL SLICKS FROM SATELLITE ALTITUDES

It is quite apparent from the limited ground coverage provided by airborne scanners that any large-scale monitoring of ocean surfaces for oil slicks must be done from satellite altitudes. NASA has already planned ERTS A and B missions with the capability to acquire multispectral images of the earth's surface on a global scale. However, the solution to the problem of locating and identifying oil slicks may not lend itself to the system already planned by NASA, and it is the purpose of the following section to investigate this possibility.

To realize NASA's goals, the ERTS A and, possibly, ERTS B missions will carry a multispectral return-beam-vidicon (RBV) TV camera system and a multispectral point scanner (MSPS). Table 4 shows the important parameters for each system.

TABLE 4. PARAMETERS FOR ERTS A AND B SYSTEMS

	RBV Multispectral Camera	MSPS
Ground Resolution (at 500 miles)	100 ft*	230 ft*
Number of Channels	3	4
Bandpass Channel No. 1	0.475-0.575 μm	0.500-0.600 μm
Bandpass Channel No. 2	0.580-0.680 μm	0.600-0.700 μm
Bandpass Channel No. 3	0.690-0.830 μm	0.700-0.800 μm
Bandpass Channel No. 4		0.800-1.200 μm

*Resolution as noted in Remote Sensing Newsletter, Texas A and M University, April 1970.

These parameters show that the optimum wavelength for detecting oil slicks (the UV, based on the data obtained from the Santa Barbara Survey), is not present in the ERTS system. However, because of the great altitudes involved, ozone absorption and Rayleigh scattering make acquisition of data in the UV region more difficult, even if the wavelength were in the ERTS sys-

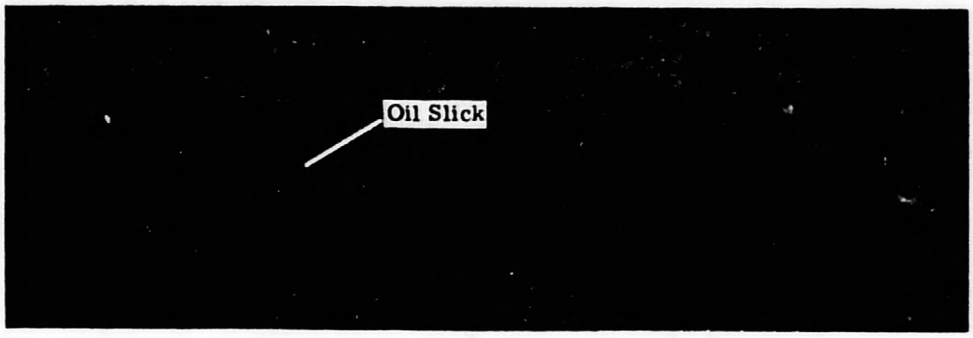

(a) March 7, 1969, 6:15 a.m. Altitude: 10,000 ft.

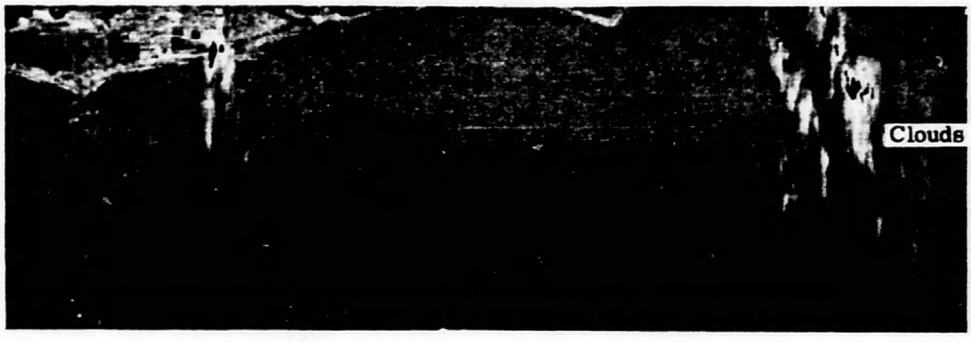

(b) March 7, 1969, 11:30 a.m. Altitude: 10,000 ft.

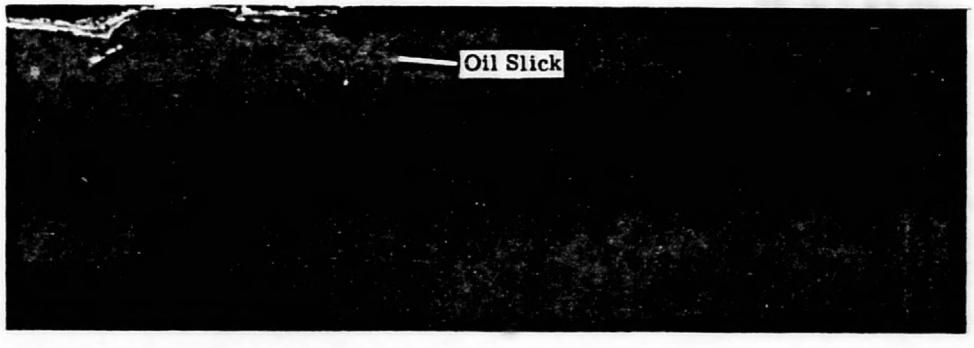

(c) March 6, 1969, 3:00 p.m. Altitude: 10,000 ft.

FIGURE 17. DRIFTING OIL SLICK NEAR SHORELINE OF SANTA BARBARA (0.40-0.44 μm)

tem, so the question becomes one of what wavelengths can be used. Of course, it would be ideal if one of the ERTS wavelengths could be used, such as Channel No. 1 of the RBV multispectral camera (see Table 4); so an analysis of the data was initiated to determine if such an implementation was possible.

The mechanism used involved employing a special computer designed at The University of Michigan. Essentially, the computer, called SPARC (SPectral Analysis and Recognition Computer), applies a decision-making rule to each resolution element of the multispectral scanner data and decides if that resolution element has the same spectral shape as a previously specified training set. This "yes" (target)—"no" (not target) output is recorded as a black and white recognition map by a film printer.

Figure 18 shows the output of SPARC for the main oil slick of Platform A during the early morning flight and for several combinations of wavelengths. The white areas in the images are those recognized by SPARC as oil. It is apparent from these data, and also from the lack of contrast observed in the red and infrared bands of Fig. 8, that the oil would be virtually impossible to recognize by means of only those bands specified in the MSPS system. Even using one of the blue channels with a red channel doesn't greatly improve the quality of the recognition map. Applying covariance to the decision-making rule considerably improves the mapping, but the setup requires a beforehand knowledge of the presence of the slick, and even then, it is doubtful anything would be seen with only those bands beyond 0.55 μm.

It may be possible to use the first channel in the RBV multispectral camera since its bandpass is very near the point where the oil-dispersant mixture starts to appear positive when compared to water. However, the poor quality of the single-channel recognition map in Fig. 8 would indicate that more than this one channel would have to be used if positive identification of the oil is desired. Since atmospheric backscatter starts to become very pronounced towards the blue end of the spectrum, the lower limit for usable wavelengths might be anywhere from 0.40 μm to 0.50 μm, so that the possibilities of detection from satellite altitude are questionable. Also, when one considers that not all oils start their absorption bands as far out in the blue region as the Santa Barbara oil, the problem becomes even more serious.

Some imagery of the slicks was taken at 10,000 ft with the multispectral scanner (Fig. 19). However, after an increase in altitude of only a factor of five, the contrast in the UV region images between oil and water is much less than in those images seen earlier. While it is encouraging to be able to see the slick in the 10,000-ft imagery, studies to determine the full effect of the atmosphere and to find the minimum ground resolution necessary for valid detection at 200 miles should be undertaken.

Figure 19 also includes an 8.0- to 14.0-μm image of the oil slick. This wavelength region does not have the atmospheric problems of the UV wavelength region, but since only the thicker

(a) Video (0.32-0.38 μm)

(b) 6-channel recognition (0.40-0.44 μm, 0.46-0.48 μm, 0.52-0.55 μm, 0.62-0.66 μm, 0.72-0.75 μm, 0.80-1.00 μm)

(c) 2-channel recognition (0.40-0.44 μm, 0.46-0.48 μm)

(d) Single-channel recognition (0.46-0.48 μm)

(e) 2-channel recognition (0.46-0.48 μm, 0.62-0.66 μm)

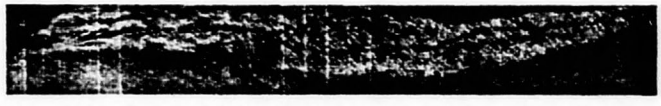

(f) 2-channel recognition with covariance (0.46-0.48 μm, 0.62-0.66 μm)

FIGURE 18. SPARC OUTPUT OF MAIN OIL LEAK.
March 7, 1969, 8:15 a.m. Altitude: 2000 ft.

parts of the oil slick are detectable, the spatial resolution problem is more difficult. The IR channel, on the other hand, would not be restricted to making observations only at certain times of the day, since angle effects would be negligible; observation at night is even possible. The fact that the slick cannot be seen during the noon flight (Fig. 19b) substantiates earlier data concerning the optimum times for observation.

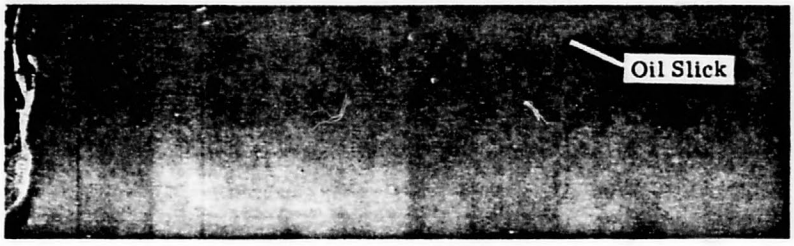

(a) March 7, 1969, 7:40 a.m., 0.40-0.44 μm

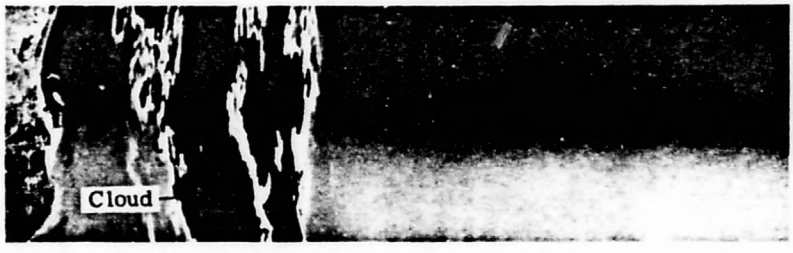

(b) March 7, 1969, 1.00 p.m., 0.40-0.44 μm

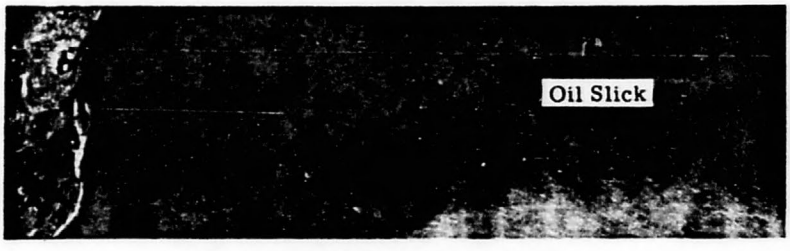

(c) March 6, 1969, 4:35 p.m., 0.40-0.44 μm

(d) March 6, 1969, 4:35 p.m., 8.0-13.5 μm

FIGURE 19. MULTISPECTRAL IMAGERY OF MAIN OIL SLICK AT AN ALTITUDE OF 10,000 ft

3
RESULTS AND CONCLUSIONS

Figures 10 through 14 indicate that the theoretical model of the oil-water interface does provide a reasonable prediction of field observations. By comparing the oil-water curves of Fig. 10, we see that 100% oil should appear light in the UV region and dark in the region from 0.42 μm to 0.57 μm. Beyond 0.57 μm, no accurate scattering data for the oil exist, so nothing

quantitative can be concluded about its behavior. Figure 8 indicates that the predicted behavior of the thick oil streamers does follow the model, at least in the first two regions mentioned above. By choosing more appropriate oil scattering coefficients beyond 0.52 μm, the curve can be made to overlay that of the water, thus satisfying the multispectral imagery. If the imagery can be used as a reference, future measurements of the oil scattering coefficients in this region (beyond 0.52 μm) should agree with those predicted from the model.

Figure 10 also indicates that the positive contrast observed for the slick in the blue wavelength region (0.40 μm—0.48 μm) cannot be caused by oil alone because the model predicts a negative contrast. Hence, apparently the dispersant, which does indicate a positive contrast to water in the blue region, must be mixing with the oil. The possibility that we are observing the dispersant alone does exist, but the extremely high UV reflectance and zero contrast in the red and near-infrared regions does not agree with the curve for the dispersant alone. However, a mixture of oil and dispersant could conceivably give the images observed from the scanner, assuming relatively low dispersant concentrations.

One disagreement with the scanner data does occur when the angle effect is considered. The multispectral imagery indicated low sun angles as the optimum time for detection of the presumed oil-dispersant mixture in the UV region, but the model predicts the reverse effect. Perhaps this can be explained by the fact that the model assumes isotropic scattering, and scattering is a major mechanism in giving the positive contrast observed in the UV. A non-isotropic scattering coefficient might explain the observed data. It is apparent, however, that more research is needed in the area of model validation.

Figures 10 through 14 also show that thickness calculations for the Santa Barbara oil are not promising in the UV region except for very thin films. Thicknesses of 0.5 mm, 0.25 mm, and 0.50 mm were all considered in the model with no change at all observed in the radiance from the UV to the near IR. For a 0.01-mm thickness, a little decrease in radiance was observed in the UV, which indicates that for very thin films (<0.01 mm) a thickness calculation might be feasible. Figure 20 shows a voltage slice of the UV data obtained on the main oil slick. Although time did not permit detailed analysis of this data, the reflectance differences between the oil-water and oil-dispersant-water surfaces occurs in discrete steps. This result supports the evidence that thickness measurements would be difficult using the UV on the Santa Barbara oil. However, the oil taken from the Santa Barbara channel is not representative of all oils. Measurements made on other oils on another contract [4] indicate that oils have widely varying absorption and scattering coefficients. It is highly probable that other oils might lend themselves to thickness determinations much more easily than the Santa Barbara oil. Of course, the potential exists for measuring thickness by means of the near-infrared or thermal wavelength regions, but more study is required here.

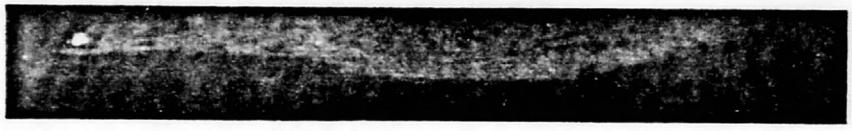

(a) Video (0.32-0.38 μm)

(b) Voltage slice

(c) Voltage slice

(d) Voltage slice

FIGURE 20. VOLTAGE SLICE OF MAIN OIL SLICK. March 7, 1969, 3:15 a.m. Altitude: 2000 ft.

The problem of locating an oil slick made up of a natural crude oil has been fairly well examined. The general conclusions drawn from the data can be summarized as follows:

(1) The optimum wavelengths to use for detection are either the UV or the thermal infrared.

(2) If the UV region is used, the data must be obtained under favorable atmospheric conditions and in the early morning or late evening when the sun is low.

(3) If the thermal region is used, it is possible that thin oil films will not be detected, and that only the thick oil streamers will appear.

(4) If oil thickness is desired, the potential for the UV is limited to thicknesses of a few microns or less. Other oils might allow thicker limits if they exhibit more suitable absorption and scattering coefficients.

(5) The potential for using the thermal regions for thickness calculations exists, but more data and modeling are required.

(6) Modeling predictions indicate that the natural oil sample used in this investigation is not suited for thickness calculations in the near-IR region. This does not rule out this region's potential for other types of oil.

4
RECOMMENDATIONS

The results of the studies carried out thus far indicate that an oil spill such as the one that occurred in the Santa Barbara Channel can be located by means of remote-sensing techniques. However, the mechanisms by which we can observe the oil are not yet fully understood, and before extension of the techniques to other oils can be carried out, further work on the model should be completed. Therefore, the following recommendations are suggested:

(1) A rigorous verification of the model should be undertaken employing closely correlated laboratory and scanner data obtained from controlled or well-documented oil spills. The problem of disagreeing angular variations must be resolved.

(2) Extension of scattering data for the Santa Barbara oil beyond 0.6 μm should be performed to determine the feasibility of employing scattering data for thickness determinations. Also, a study of the uniformity of scattering effects for various petroleum products by obtaining scattering data from other oil slicks is desirable.

(3) A thermal model should be developed to examine the possibility of locating oil slicks and determining their thickness using the 8.0- to 13.5-μm region.

(4) A simulation of high-altitude imagery should be made from the 10,000-ft imagery obtained during the Santa Barbara Survey. This would be necessary to determine minimum spatial resolution for a satellite system to detect an oil slick of the size observed in the Santa Barbara Channel.

(5) A more detailed study of the ERTS A and B systems should be made with major emphasis on the optimum wavelengths to use and the atmospheric problems to be encountered. Also, an investigation of a laser system for locating oil slicks should be investigated, especially in connection with potential nighttime detection.

Appendix I
A SPECULAR AND DIFFUSE REFLECTANCE MODEL OF OIL ON THE SEA SURFACE

The work on the reflectance model which appears in this appendix was performed under Coast Guard Contract No. DOT-CG-92580-A, and taken verbatim from pp. 2-5 and pp. 159-165 of the Final Report for that contract. However, because a new technique to obtain scattering coefficients (Appendix III) was derived from the model, it was considered necessary to include the whole model for continuity.

I.1. MODEL GEOMETRY AND NOMENCLATURE

Let us divide the power into organized collimated power, which can produce specularly reflected images, and diffuse power, caused by isotropic particulate scatterers. That power which remains collimated may be treated by geometrical optics. It is assumed, however, that the power which is scattered may never return to the collimated direction; thus, initially collimated power which penetrates a scattering medium tends to disappear into diffuse forms and into heat. The diffuse power must be solely from the incident organized power. There are no other power sources.

The model of the oil slick consists of three regions of material: region 1 is air; region 2 is oil; region 3 is sea water. The configuration is considered to consist of uniform plane layers of material with the top of the oil layer at $x = 0$. Positive values of x are up into the air region from this surface. The oil-sea junction is at $x = -h$, making the oil-film thickness h. The bottom of the sea layer is at $x = -\infty$. The downward-flowing spectral irradiance is designated by E^- and the upward-flowing spectral irradiance by E^+. The position and region for which the spectral irradiance is given is denoted by $E^+(x,i,d)$ for upward-flowing spectral irradiance at x in the i-th region and of the diffuse type. $E^+(x,i,s)$ is for the upward-flowing spectral irradiance at x in the i-th region and of the specular or organized type. M^+ denotes the exitance (net power) reflected as a result of all the E^- and E^+ irradiances. M^+ is the quantity which is observed by sensing devices. See Fig. 21 for illustration. The division of power flow into specular and diffuse types is necessary because scattered power within an oil layer will be partially trapped. Scattered power incident on the oil side of the surface can be incident at angles greater than the critical angle. Such power will be totally reflected back into the oil layer. Specular power can never be trapped in this way. If specular power can enter the layer, then the power which remains specular can never be incident on the oil side at angles greater than the critical angle.

Each region may be characterized by a spectral absorption coefficient, α, and a spectral scattering coefficient, σ. In region 1 (air), it is assumed that these properties are all included

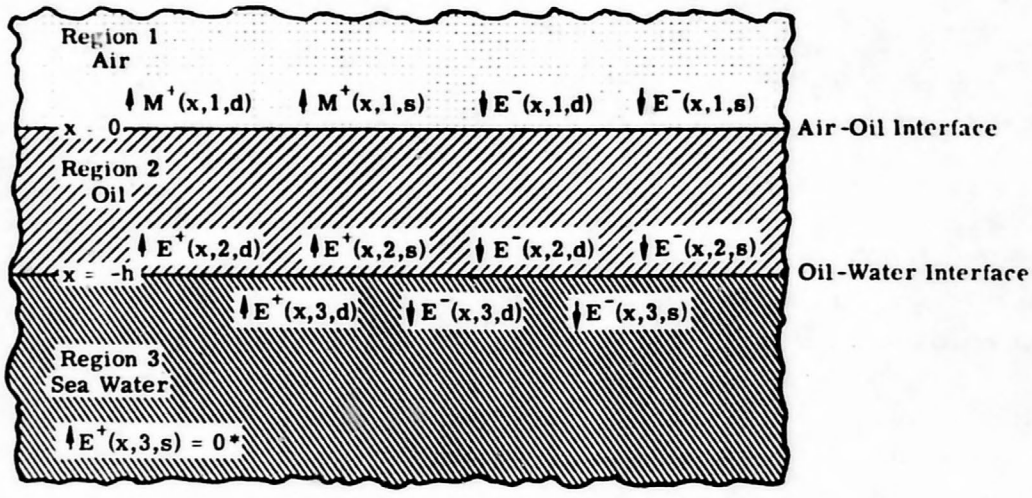

*No specular reflectance occurs below oil-water interface.

FIGURE 21. POWER FLOW IN AIR-OIL-WATER LAYERED SYSTEM

in the irradiance, $E^-(0,1,s)$, and need not be considered further. However, region 2 is characterized by absorption and scattering coefficients $\alpha(2)$ and $\sigma(2)$, and region 3 by $\alpha(3)$ and $\sigma(3)$. At the boundaries, we may expect reflections of power which depend upon the type of power flow and the nature of the boundary materials. Referring to Fig. 21, note that $M^+(x,1,d)$ and $M^+(x,1,s)$ are the diffuse and specular exitances which represent net reflected power after absorption and scattering within the oil, water, and air.

The quantity of fundamental interest is the reflectance, i.e., the ratio of net reflected power to incident power, $\frac{M^+(0,1,s)}{E^-(0,1,s)}$ for specular and $\frac{M^+(0,1,d)}{E^-(0,1,s)}$ for diffuse. The reflectances resulting from the various media are determined from the Fresnel equations. These individual reflectances are designated by $\rho(i,j,s)$ or $\rho(i,j,d)$. Thus, $\rho(i,j,d)$ is the average reflectance of diffuse power flowing in region i toward the region-j junction, and $\rho(i,j,s)$ is the specular reflectance at some angle of incidence θ for specular power flowing in region i toward the region-j junction. Note that the properties of these reflectances are such that

$$\rho(i,j,s) = \rho(j,i,s)$$

but

$$\rho(i,j,d) \neq \rho(j,i,d)$$

and

$$\rho(i,j,s) \neq \rho(i,j,d)$$

Because of critical angle trapping, the reflectance of diffuse power is necessarily a hemispherical average of the specular reflectance. For example, $\rho(i,j,d) = \bar{\rho}(i,j,s)$, where the bar indicates hemispherical average, and where the index of refraction of region i is less than that of region j. Then also, under these same conditions

$$\rho(j,i,d) = \left\{ 1 - [1 - \rho(i,j,d)] \frac{n_1^2}{n_j^2} \right\}$$

where n_i = the index of refraction of region i

n_j = the index of refraction for region j

The hemispherical average reflectance is found from the specular reflectance by

$$\bar{\rho}(i,j,s) = 2\pi \int_0^{\pi/2} \rho(i,j,s,\theta) \sin\theta \cos\theta \, d\theta$$

when the index of refraction in the i-th region is less than that in the j-th region. Rather than measuring $\rho(i,j,s,\theta)$, it is just as well to depend upon Fresnel's equations relating this quantity to the refractive indices.

I.2. MATHEMATICAL PROCEDURES

I.2.1. THE DIFFERENTIAL EQUATIONS OF FLOW

For every region i, the diffuse power flow is given by

$$\frac{dE^-(x,i,d)}{dx} = 2(\alpha + \sigma)E^-(x,i,d) - 2\sigma E^+(x,i,d) - \sigma E^-(x,i,s) - \sigma E^+(x,i,s) \qquad (1)$$

$$\frac{dE^+(x,i,d)}{dx} = -2(\alpha + \sigma)E^+(x,i,d) + 2\sigma E^-(x,i,d) + \sigma E^-(x,i,s) + \sigma E^+(x,i,s) \qquad (2)$$

The factor 2 appearing in front of these diffuse E terms is necessary because the energy-mean ray of a Lambertianly diffuse bundle of rays flowing across the interval dx will travel at an angle of 60^o from the x direction; thus, it will encounter twice as many scattering and absorbing interactions (sec 60^o dx = 2 dx). The specular power flow is given by

$$\frac{dE^+(x,i,s)}{dx} = -(\alpha + 2\sigma)E^+(x,i,s) \qquad (3)$$

$$\frac{dE^-(x,i,s)}{dx} = (\alpha + 2\sigma)E^-(x,i,s) \qquad (4)$$

The scattering of specular power flowing in a given direction removes such power at twice the rate of diffuse-power loss; this occurs because both forward scattering and backscattering dis-

sipate specular power, but only backscattering removes diffuse power from its appropriate category. Forward-scattered diffuse power is still diffuse-power flow in the initial flow direction. Thus, the extinction coefficient of specular power is $\kappa = (\alpha + 2\sigma)$.

Relations (3) and (4) yield for solutions

$$E^+(x,i,s) = C_o e^{-\kappa x} \tag{5}$$

$$E^-(x,i,s) = D_o e^{+\kappa x} \tag{6}$$

The general solutions of (1) and (2) have the form

$$E^- = A(1 + b)e^{gx} + B(1 - b)e^{-gx} + Ce^{-\kappa x} + De^{\kappa x} \tag{7}$$

$$E^+ = A(1 - b)e^{gx} + B(1 + b)e^{-gx} + Ee^{-\kappa x} + Fe^{\kappa x} \tag{8}$$

The last two terms on the right of (7) and (8) will involve the input specular power. Substitution of (5), (6), (7), and (8) into (1) and (2) yields:

$$\frac{\partial E^-}{\partial x} = 2(\alpha + \sigma)[A(1 + b)e^{gx} + B(1 - b)e^{-gx} + Ce^{-\kappa x} + De^{\kappa x}] - 2\sigma[A(1 - b)e^{gx}$$

$$+ B(1 + b)e^{-gx} + Ee^{-\kappa x} + Fe^{\kappa x}] - \sigma D_o e^{\kappa x} - \sigma C_o e^{-\kappa x}$$

$$= A(1 + b)ge^{gx} + B(1 - b)(-g)e^{-gx} - \kappa Ce^{-\kappa x} + \kappa De^{\kappa x}$$

$$\frac{\partial E^+}{\partial x} = -2(\alpha + \sigma)[A(1 - b)e^{gx} + B(1 + b)e^{-gx} + Ee^{-\kappa x} + Fe^{\kappa x}] + 2\sigma[A(1 + b)e^{gx}$$

$$+ B(1 + b)e^{-gx} + Ce^{-\kappa x} + De^{\kappa x}] + \sigma D_o e^{\kappa x} + \sigma C_o e^{-\kappa x}$$

$$= A(1 - b)ge^{gx} + B(1 + b)(-g)e^{-gx} - \kappa Ee^{-\kappa x} + \kappa Fe^{\kappa x}$$

Equating coefficients and solving for b and g:

$$2(\alpha + \sigma)(1 + b) - 2\sigma(1 - b) = (1 + b)g \rightarrow g = 2(\alpha + \sigma) - 2\sigma\left(\frac{1 - b}{1 + b}\right)$$

$$2(\alpha + \sigma)(1 - b) - 2\sigma(1 + b) = (1 - b)(-g) \rightarrow g = -2(\alpha + \sigma) + 2\sigma\left(\frac{1 + b}{1 - b}\right)$$

which gives

$$b = \sqrt{\alpha/\kappa}$$

$$g = 2\sqrt{\alpha\kappa}$$

Equating coefficients for C, D, E, and F gives

$$2(\alpha + \sigma)C - 2\sigma E - \sigma C_o = -\kappa C \rightarrow E = \frac{(3\alpha + 4\sigma)C - \sigma C_o}{2\sigma}$$

$$2(\alpha + \sigma)D - 2\sigma F - \sigma D_o = \kappa D \rightarrow F = \frac{\sigma D - \sigma D_o}{2\sigma}$$

$$-2(\alpha + \sigma)E + 2\sigma C + \sigma C_o = -\kappa E \rightarrow E = \frac{2\sigma C + \sigma C_o}{\alpha}$$

$$-2(\alpha + \sigma)F + 2\sigma D + \sigma D_o = \kappa F \rightarrow F = \frac{2\sigma D + \sigma D_o}{3\alpha + 4\sigma}$$

Solution gives

$$C = -fC_o$$

$$D = -3fD_o$$

$$E = -3fC_o$$

$$F = -fD_o$$

where $f = \frac{\sigma}{8\sigma - 3\kappa}$. The above relationships hold for each region.

I.2.2. BOUNDARY CONDITIONS FOR SPECULAR POWER FLOW

The boundary conditions for the organized specular power are applied first to determine D_o and C_o. For the case of oil at x = 0, sea at x = -h, and sea bottom at x = -∞, the values of D_o and C_o are

$$D_o = \frac{E^-(0,1,s)[1 - \rho(1,2,s)]}{\left[1 - \rho(2,1,s)\rho(2,3,s)e^{-2\kappa h \sec \theta_i}\right]}$$

where θ_i is the angle of refraction for a given θ incident angle at the air-oil surface, and

$$C_o = \rho(2,3,s)D_o e^{-2\kappa h \sec \theta_i}$$

The specular exitance, $M^+(0,1,s)$ is then

$$M^+(0,1,s) = E^+(0,2,s)[1 - \rho(1,2,s)] + E^-(0,1,s)\rho(1,2,s)$$

Calculation of the ratio $M^+(0,1,s)/E^-(0,1,s)$ yields the overall specular reflectance of the model, ρ(model, s).

$$\rho(\text{model, s}) = \frac{[1 - \rho(1,2,s)]^2 \rho(2,3,s) e^{-2\kappa h \sec \theta_i}}{1 - \rho(2,1,s)\rho(2,3,s) e^{-2\kappa h \sec \theta_i}} + \rho(1,2,s)$$

I.2.3. BOUNDARY CONDITIONS FOR DIFFUSE POWER FLOW

The boundary conditions for diffuse power flow are as follows:

At $x = 0$

$$E^-(0,2,d) = \rho(2,1,d)E^+(0,2,d) \tag{9}$$

and

$$M^+(0,1,d) = [1 - \rho(2,1,d)]E^+(0,2,d) \tag{10}$$

At $x = -h$

$$E^+(-h,2,d) = \rho(2,3,d)E^-(-h,2,d) + E^+(-h,3,d)[1 - \rho(3,2,d)] \tag{11}$$

$$E^-(-h,3,d) = [1 - \rho(2,3,d)]E^-(-h,2,d) + E^+(-h,3,d)\rho(3,2,d) \tag{12}$$

At $x = -\infty$

$$E^+(-\infty,3,d) = E^-(-\infty,3,d) = 0 \tag{13}$$

In working with these boundary conditions, the following short notation will be used. For region 2, the constants A, B, D, E, α, σ, and κ appear without modifying marks. For region 3, the sea water, these constants appear with a prime; thus, A', B', D' . . . , etc. are the constants for region 3.

Beginning in region 3, the upward-flowing specular power must be zero everywhere, since there is no specular reflection below the sea surface in this model. Thus, $C'_o = 0$ from (5) and, therefore,

$$C' = E' = 0$$

$$D' = -3f'D'_o$$

$$F' = -f'D'_o$$

Further, at $x = -\infty$, the diffuse power (13) must eventually disappear entirely so that $B' = 0$. Therefore, the solutions (7) and (8) for region 3 reduce to

$$E^-(x,3,d) = A'(1 + b')e^{\beta' x} + D'e^{\kappa' x} \tag{14}$$

$$E^+(x,3,d) = A'(1 - b')e^{\beta' x} + F'e^{\kappa' x} \tag{15}$$

The constant D_o' is directly related to D_o through the specular reflection factors at the (2, 3) boundary.

$$D_o' = [1 - \rho(2,3,s)]D_o e^{-(\kappa-\kappa')h \sec \theta_i}$$

Now, applying general solutions (7) and (8) for region 2 and (14) and (15) for region 3 to the boundary conditions at x = -h, as shown in relations (11) and (12), we obtain

$$[A(1 - b)e^{-gh} + B(1 + b)e^{gh} + Ee^{\kappa h} + Fe^{-\kappa h}] = \rho(2,3,d)[A(1 + b)e^{-gh} + B(1 - b)e^{gh} + \ldots$$
$$+ Ce^{\kappa h} + De^{-\kappa h}] + [1 - \rho(3,2,d)][A'(1 - b')e^{-g'h} + F'e^{-\kappa' h}] \quad (16)$$

$$[A'(1 + b')e^{-g'h} + D'e^{-\kappa' h}] = [1 - \rho(2,3,d)][A(1 + b)e^{-gh} + B(1 - b)e^{gh} + Ce^{\kappa h} + \ldots$$
$$+ De^{-\kappa h}] + \rho(3,2,d)[A'(1 - b')e^{-g'h} + F'e^{-\kappa' h}] \quad (17)$$

Applying the solutions (7) and (8) for region 2 to the x = 0 boundary conditions of (9) and (10), we obtain

$$[A(1 + b) + B(1 - b) + C + D] = \rho(2,1,d)[A(1 - b) + B(1 + b) + E + F] \quad (18)$$

$$M^+(0,1,d) = [1 - \rho(2,1,d)][A(1 - b) + B(1 + b) + E + F] \quad (19)$$

The constants b', g', κ' are found from known properties of sea water; b, g, and κ are found from known properties of the oil layer. The reflectances are determined from refractive indices. The constants C_o and D_o are derived from these reflectances and the input specular irradiance, $E^-(0,1,s)$. Thus, four unknown quantities, A', A, B, $M^+(0,1,d)$ remain to be found from the four relations given in (16), (17), (18) and (19). Since $M^+(0,1,d)$ is the diffuse, upward-flowing exitance which is to be intercepted by the remote sensing instrument, we will solve directly only for $M^+(0,1,d)$.

The four simultaneous equations (16) through (19) may be written in shorthand notation as:

$$\begin{aligned} K_{11}A' + K_{12}A + K_{13}B + K_{14}M^+ &= J_1 \\ K_{21}A' + K_{22}A + K_{23}B + K_{24}M^+ &= J_2 \\ K_{31}A' + K_{32}A + K_{33}B + K_{34}M^+ &= J_3 \\ K_{41}A' + K_{42}A + K_{43}B + K_{44}M^+ &= J_4 \end{aligned} \quad (20)$$

where $K_{11} = -[1 - \rho(3,2,d)](1 - b')e^{-g'h}$

$K_{12} = [(1 - b) - \rho(2,3,d)(1 + b)]e^{-gh}$

$$K_{13} = [(1 + b) - \rho(2,3,d)(1 - b)]e^{gh}$$

$$K_{14} = 0$$

$$K_{21} = [(1 + b') - \rho(3,2,d)(1 - b')]e^{-g'h}$$

$$K_{22} = -[1 - \rho(2,3,d)](1 + b)e^{-gh}$$

$$K_{23} = -[1 - \rho(2,3,d)](1 - b)e^{gh}$$

$$K_{24} = 0$$

$$K_{31} = 0$$

$$K_{32} = (1 + b) - \rho(2,1,d)(1 - b)$$

$$K_{33} = (1 - b) - \rho(2,1,d)(1 + b)$$

$$K_{34} = 0$$

$$K_{41} = 0$$

$$K_{42} = -[1 - \rho(2,1,d)](1 - b)$$

$$K_{43} = -[1 - \rho(2,1,d)](1 + b)$$

$$K_{44} = 1$$

$$J_1 = D_o\left\{f[3 - \rho(2,3,d)]e^{\kappa h(1-2\sec\theta_i)} + f[1 - 3\rho(2,3,d)]e^{-\kappa h} + \cdots + f'[1 - \rho(3,2,d)][1 - \rho(2,3,s)]e^{-[\kappa' + (\kappa - \kappa')\sec\theta_i]h}\right\}$$

$$J_2 = D_o\left\{-f[1 - \rho(2,3,d)]\rho(2,3,s)e^{\kappa h(1-2\sec\theta_i)} - 3f[1 - \rho(2,3,d)]^{-\kappa h} + \cdots + f'[3 - \rho(3,2,d)][1 - \rho(2,3,s)]e^{-[\kappa' + (\kappa - \kappa')\sec\theta_i]h}\right\}$$

$$J_3 = D_o\left\{f[1 - 3\rho(2,1,d)]e^{-2\kappa h\sec\theta_i} + f[3 - \rho(2,1,d)]\right\}$$

$$J_4 = D_o\left\{-f[1 - \rho(2,1,d)] - 3f\rho(2,3,s)[1 - \rho(2,1,d)]e^{-2\kappa h\sec\theta_i}\right\}$$

Using Cramer's rule for simultaneous solution by determinants, it is immediately seen from (20) that the denominator of M^+ is the 3×3 determinant (with $K_{44} = 1$),

$$\begin{vmatrix} K_{11} & K_{12} & K_{13} \\ K_{21} & K_{22} & K_{23} \\ 0 & K_{32} & K_{33} \end{vmatrix}$$

While the numerator of M^+ is the 4 × 4 determinant,

$$\begin{vmatrix} K_{11} & K_{12} & K_{13} & J_1 \\ K_{21} & K_{22} & K_{23} & J_2 \\ 0 & K_{32} & K_{33} & J_3 \\ 0 & K_{42} & K_{43} & J_4 \end{vmatrix}$$

Substitution of the appropriate values will yield the diffuse spectral exitance from a specular source.

To avoid further complications, we will assume that the scattered exitance is Lambertian in distribution, so that the diffuse spectral radiance $L(d) = M^+/\pi$. Further, we should consider sky light as providing an average spectral radiance independent of polar angle so that $\rho(1,2,s)$ for sky light can be replaced by its hemispherical average

$$\bar{\rho}(1,2,s) = 2\pi \int_0^{\pi/2} \rho(1,2,s,\theta) \sin\theta \cos\theta \, d\theta$$

Likewise, $\rho(3,2,s)$ is replaced by $\bar{\rho}(3,2,s)$. Since $\rho(3,2,s) = \rho(2,3,s)$, then $\bar{\rho}(3,2,s) = \bar{\rho}(2,3,s)$. Trapping by critical-angle reflection will not occur for specular power. The diffuse exitance contributed by direct sunlight may be treated in the same fashion by using the solar angle in computing D_o, $\rho(1,2,s)$, and $\rho(2,1,s)$.

Appendix II
LABORATORY MEASUREMENTS OF EXTINCTION COEFFICIENTS, SCATTERING COEFFICIENTS, AND INDEX OF REFRACTION

By considering Maxwell's equation for a conducting medium, one can show that the transverse fields being propagated in the $\vec{k}$ direction may be represented as:

$$\vec{E}(\vec{r}) = \vec{E}_o e^{-i\left(\omega t - \frac{\omega}{c} N \hat{k} \cdot \vec{r}\right)} \tag{21}$$

where $\vec{E}(r)$ = electric field vector at position r

$|\vec{E}_o|$ = the amplitude of the wave

ω = the angular frequency of the wave

c = the velocity of light in vacuum

N = the complex index of refraction

$\hat{k}$ = a unit vector in the direction of propagation of the wave

t = time

$\vec{r}$ = a position vector

The complex index of refraction is now defined as:

$$N = n + i\frac{c}{2\omega}\alpha = n + \frac{i\alpha\lambda}{4\pi} \tag{22}$$

where n is now the real index of refraction representing the ratio of the speed of light in vacuum to the speed of light in the medium. The constant α is called the absorption coefficient and is dependent on wavelength λ.

Substituting the expression for N[Eq. (22)] in Eq. (21) yields

$$\vec{E}(\vec{r}) = \vec{E}_o e^{-i\left[\omega t - \frac{\omega}{c}\left(n + i\frac{c}{2\omega}\alpha\right)\hat{k}\cdot\vec{r}\right]}$$

$$= \vec{E}_o e^{-\frac{\alpha}{2}\hat{k}\cdot\vec{r}} e^{-i\left[\omega t - \frac{\omega}{c}n\hat{k}\cdot\vec{r}\right]}$$

Since the intensity, I, is proportional to the amplitude squared of the electric field vector, this may be written in terms of intensity as:

$$I = I_o e^{-\alpha\hat{k}\cdot\vec{r}}$$

$$= I_o e^{-\alpha z}$$

where $z = \hat{k}\cdot\vec{r}$ = the distance traveled by the wave in the medium

I_o = the incident intensity entering the medium

I = the intensity a distance z within the medium

Therefore, the absorption coefficient represents the distance traveled in the medium which produces an attenuation of 1/e. This exponential decay corresponds physically to energy supplied to electronic transitions for ultraviolet and visible radiation and to molecular-rotational and molecular-vibrational transitions for infrared radiation.

If the material through which the radiation is being propagated contains particulate matter, some energy will be scattered away from this propagation direction. On the macroscopic scale, this appears as an attenuation of the specular intensity. In practice, it is difficult, if not impossible, to completely differentiate between pure scattering and pure absorption. Just as for the absorption coefficient, the scattering coefficient σ is defined as that distance traveled in the material which decreases the incident intensity by a factor of 1/e and is caused solely by scattering effects. Therefore, the total attenuation of radiation being propagated through a scattering and absorbing medium may be characterized by an extinction coefficient κ which is the sum of these scattering and absorption coefficients.

The intensity at some distance z within this medium is then given in terms of the incident intensity by:

$$I = I_o e^{-\kappa z} \tag{23}$$

with I, I_o, and z as defined above.

II.1. EXTINCTION COEFFICIENTS

II.1.1. THEORY

In practice, measurement of the extinction coefficient of a liquid sample necessitates placing the liquid in a cell with windows of an appropriate material, which means that a beam of light transmitted through the cell will be affected not only by the optical properties of the sample but also by those of the windows.

If one considers a three-layer cell consisting of a sample between two windows as shown in Fig. 22, an energy balance may be written for the system. The incident beam of intensity, I_o, will be partially reflected and partially transmitted at the front window surface. If the fraction of the incident beam which is reflected is denoted by $\rho_{A,1}$, then the transmitted portion of the incident beam is necessarily $(1 - \rho_{A,1})$. Then, as the beam propagates through the window material, it experiences an attenuation given by Eq. (23) where κ and z are the extinction coefficient and thickness of the window material respectively. At the oil-window interface another partial reflection and partial transmission takes place. Again the transmitted portion will be

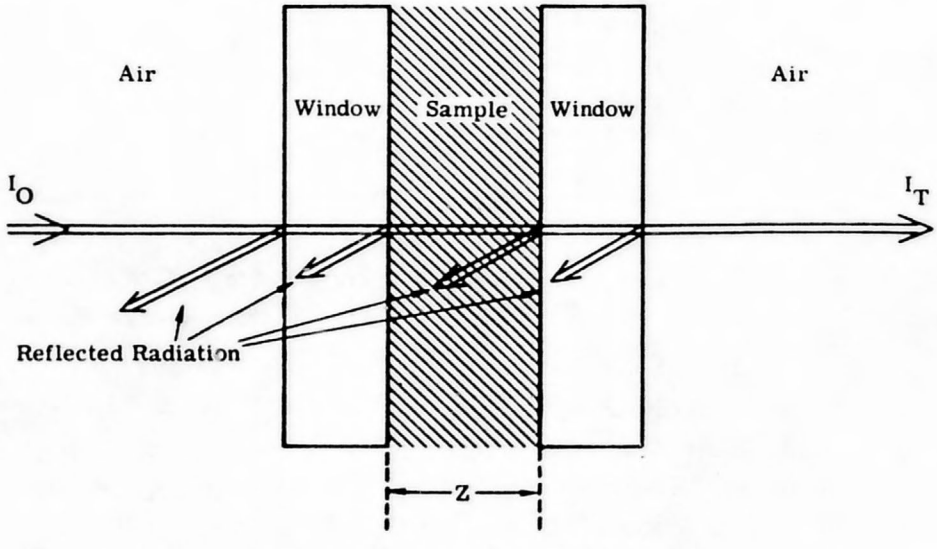

FIGURE 22. THREE LAYER CELL

given by $(1 - \rho_{1,2})$. Proceeding in this manner through the entire cell, one obtains for the relationship between the transmitted and incident intensities:

$$I_T = I_o(1 - \rho_{A,1})^2(1 - \rho_{1,2})^2 e^{-\kappa_2 z_2} e^{-2\kappa_1 z_1} \tag{24}$$

where $\rho_{A,1}$ = the reflection coefficient for the interface between air and the window

$\rho_{1,2}$ = the reflection coefficient for the interface between the window and sample

κ_1 = the extinction coefficient of the window material

κ_2 = the extinction coefficient of the sample

z_1 = path length of the radiation through the window

z_2 = path length of the radiation through the sample

If a similar expression is written for an identical cell except for a different sample thickness z_2, the ratio of this expression to that given above is:

$$\frac{(I_T/I_o)}{(I'_T/I_o)} = \frac{(1 - \rho_{A,1})^2(1 - \rho_{1,2})^2 e^{-\kappa_2 z_2} e^{-2\kappa_1 z_1}}{(1 - \rho_{A,1})^2(1 - \rho_{1,2})^2 e^{-\kappa_2 z'_2} e^{-2\kappa_1 z_1}}$$

It will be noticed that all the terms depending on the optical properties of the windows cancel. If this is then solved for κ_2, one obtains

$$\kappa_2 = \frac{\ell n\,(I_T/I_o) - \ell n\,(I'_T/I_o)}{(z'_2 - z_2)} \tag{25}$$

This, then, allows the calculation of κ_2 if one knows the thickness of the two layers (z_1 and z_2) and the intensity transmitted through them.

II.1.2. EXPERIMENTAL PROCEDURE AND RESULTS

Measurements of the extinction coefficient, κ, were performed on a Beckman DK-2 spectrophotometer in the 0.24-μm to 2.6-μm region and on a Perkin-Elmer Model 21 spectrophotometer in the 2.0-μm to 14.0-μm region. Schematic diagrams of these instruments are shown in Figs. 23 and 24.

In making the extinction coefficient measurements, conventional liquid-absorption cells were employed. These cells consist of matched windows separated by a spacer of known thickness, as shown in Fig. 25. Because of the transmission requirements in the various regions of the spectrum, fused-quartz windows were used in the Beckman cells, while Irtran-II windows were used in the Perkin-Elmer cells.

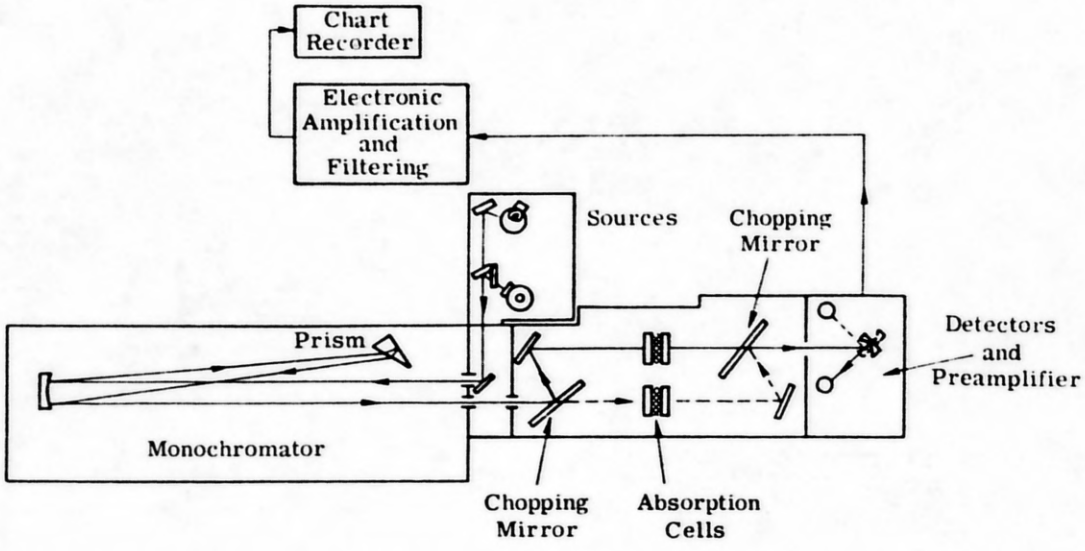

FIGURE 23. BECKMAN DK-2 WITH TRANSMISSION ATTACHMENT

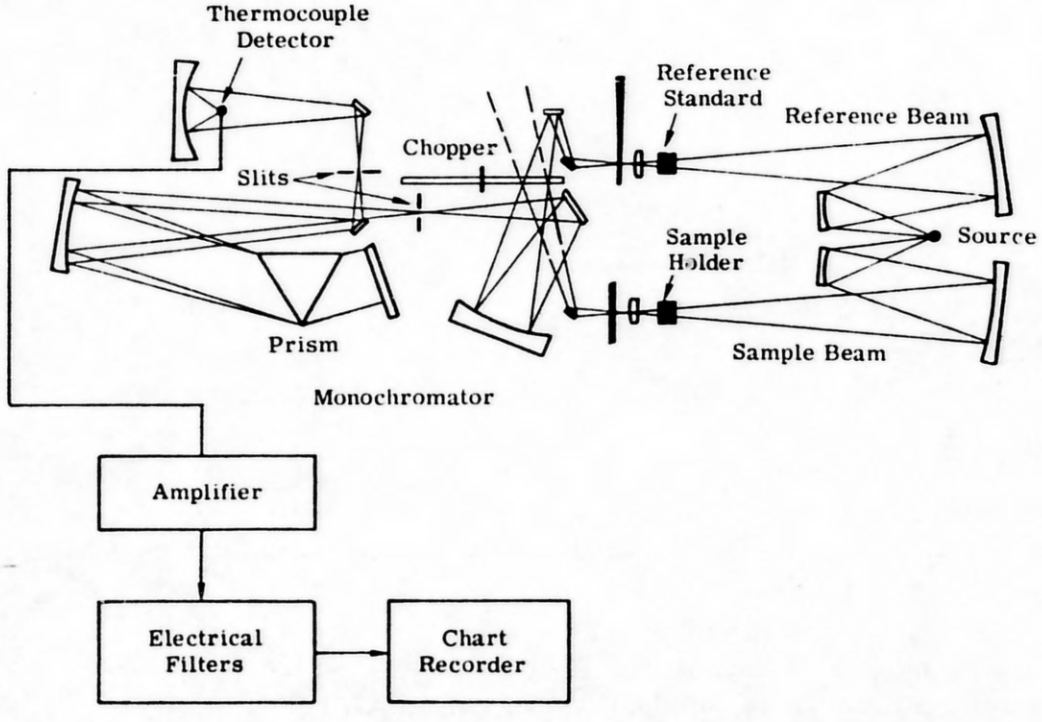

FIGURE 24. PERKIN-ELMER MODEL 21 SPECTROPHOTOMETER

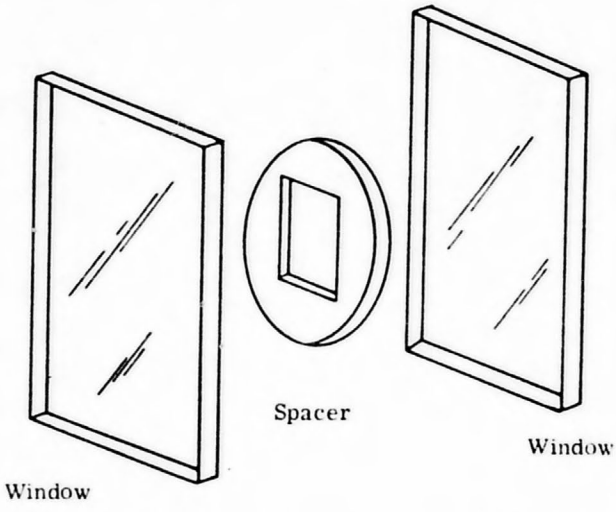

FIGURE 25. ABSORPTION CELL ARRANGEMENT

When filled with a sample, these absorption cells comprise a three-layer dielectric cell; Eq. (24) above applies. Since the Beckman and Perkin-Elmer spectrophotometers are ratio-recording instruments, if the sample cell is run against an aperture of identical dimensions, the ratio (I_T/I_o) will be the result of a single measurement on these instruments. Therefore, if measurements are made for two different thicknesses of a particular sample employing the same or identical cells, the extinction coefficient of the sample may be calculated from Eq. (25).

Extinction coefficient measurements were made for pure dispersant, Santa Barbara crude oil, and a 40:1 mixture of sea water and dispersant. Plots of the resultant data are presented in Figs. 26 through 28.

II.2. SCATTERING COEFFICIENT

II.2.1. THEORY

Both scattering and absorption follow exponential laws and both macroscopically appear as an attenuation of input specular power. It is this similarity which makes isolation and measurement of either of these mechanisms an extremely difficult task. In the present work, an indirect method of measuring the scattering coefficient was devised based on the model discussed in Appendix I. Although it may seem invalid to employ the same model for gathering data and for analyzing it, we feel justified in the case of scattering. The reason is that the model assumes isotropic scattering, and although this assumption is not completely valid, it is a reasonable and necessary first approximation. In using this model to obtain scattering coefficients, the data will be more compatible with the assumption of isotropic scattering and the data should at least partially compensate for inaccuracies produced by it.

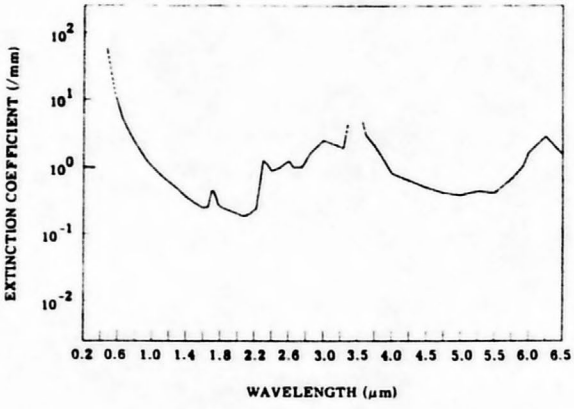

FIGURE 26. EXTINCTION COEFFICIENT—SANTA BARBARA OIL

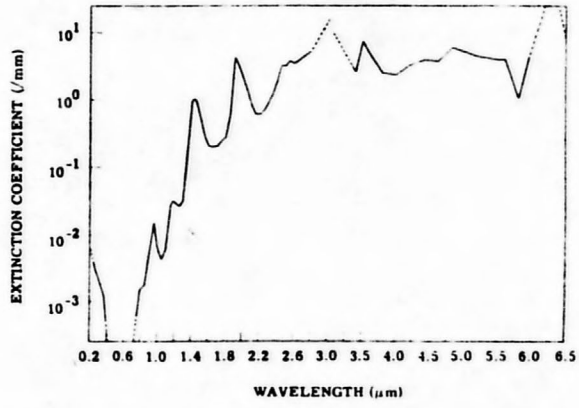

FIGURE 27. EXTINCTION COEFFICIENT—SEA WATER

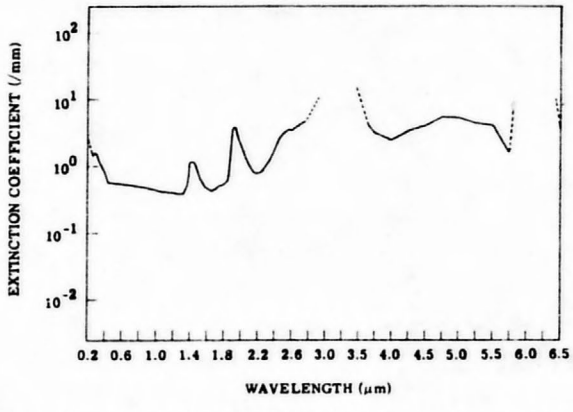

FIGURE 28. EXTINCTION COEFFICIENT—40:1 MIXTURE OF SEA WATER AND DISPERSANT

The method employed to measure the scattering coefficient was based on measurements of the distribution of radiation reflected from an optically thick layer of the sample. In the model, this is represented by two semi-infinite layers of the sample and air meeting at x = 0 as shown in Fig. 43. All optical parameters are defined in the same manner as those of Appendix I. Following the same mathematical procedure, one may obtain an expression for the diffuse reflectance of the system:

$$\frac{M^{+}(0,1,d)}{E^{-}(0,1,s)} = \frac{1}{2 - 3\left[\frac{\alpha}{\sigma}\right]}[1 - \rho(2,1,d)][1 - \rho(1,2,s)]\left\{\frac{[3 - \rho_{(2,1,d)}]}{\frac{[1 + 2(\sigma/\alpha)]^{1/2} + 1}{[1 + 2(\sigma/\alpha)]^{1/2} - 1} - \rho_{(2,1,d)}} - 1\right\} \quad (26)$$

A full treatment of the derivation of this expression is found in Appendix III. Since all the reflection coefficients may be calculated if the index of refraction and the incidence angle at the sample surface are known, the only unknown in the expression on the right is the ratio of the absorption coefficient to the scattering coefficient (α/σ). Therefore, measurement of the diffuse reflectance for an optically thick layer allows one to evaluate this ratio. As discussed in the previous section, the extinction coefficient κ had been determined, and since

$$\kappa = \alpha + 2\sigma$$

in the language of the model, one may combine these results with values of (α/σ) and obtain values for α or σ alone. If one defines R as the ratio (α/σ) then

$$\alpha = R\sigma$$

and

$$\alpha = \kappa - 2\sigma$$

therefore,

$$\sigma = \kappa/(2 + R) \tag{27}$$

It should be noted that (α/σ) appears in three terms of equation (26). This makes it impossible to solve this equation directly for (α/σ). In fact, the first term appears to have a singularity at $\sigma = 3\alpha/2$. In order to investigate the feasibility of mathematically fitting this equation to experimental data, a CDC-1604 computer was used to produce plots of $M^+(0,1,d)/E^-(0,1,s)$ versus (α/σ). It was found that equation (26) is a monotonically increasing function of (α/σ) and that no singularity exists at $\sigma = 3\alpha/2$. It was therefore practical to determine (α/σ) by fitting this function to experimental values of $M^+(0,1,d)/E^-(0,1,s)$.

II.2.2. EXPERIMENTAL PROCEDURE AND RESULTS

As discussed above, a measurement of the ratio of the diffuse exitance to the incident specular power $M^+(0,1,d)/E^-(0,1,s)$ allows one to determine the scattering coefficient using Eqs. (26) and (27). To determine this ratio, the distribution of radiation reflected from an optically thick layer of the sample was measured on an automated gonioreflectometer developed for this specific purpose at the Willow Run Laboratories under Air Force sponsorship [Contracts AF 33(615)-3924 and F33615-68-C-1281]. Figure 29 shows this apparatus as used for measurements on an oil sample. Because the time required for setup, data collection, and data reduction made measurements throughout the visible spectrum impractical, scattering measurements were limited to the ultraviolet, blue, and green regions of the spectrum. These regions were chosen because preliminary, qualitative investigations indicated that these were the regions in which significant scattering occurred.

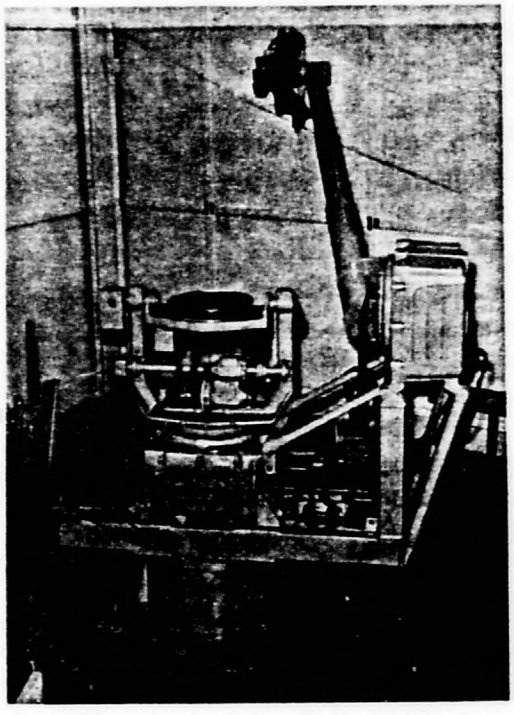

FIGURE 29. GONIOREFLECTOMETER

In setting up the gonioreflectometer, it was necessary to use broadband radiation because the spectral regions of interest were in low response areas of the detector, and narrower bandwidths reduced the energy to a stage where reasonable measurements could not be made. The bands finally decided upon were 0.35 μm to 0.39 μm, 0.38 μm to 0.47 μm, and 0.54 μm to 0.57 μm.

The output from the goniometer scans were reflection distribution functions depending on the azimuth and polar angles of the source and receiver. Graphs of these functions are presented in Figs. 30 through 35 for the oil and a 40 to 1 mixture of sea water and dispersant.

To obtain the desired ratio, $M^{+}(0,1,d)/E^{-}(0,1,s)$, from this data, azimuthal symmetry was assumed, and a numerical integration of the curves made using Willow Run Laboratories CDC-1604 computer. This resulted in a total reflectance for the samples including both diffuse and specular components. From knowledge of the refractive indices of the samples, the specular component was mathematically subtracted leaving only the desired diffuse reflectance $M^{+}(0,1,d)/E^{-}(0,1,s)$. These values were then used in Eq. (26), and the CDC-1604 computer was

employed to fit this equation to the experimental data. Equation (27) then gave values of the scattering coefficient σ.

This method is based on measurements made on an optically thick layer. Oil layers of even a few centimeters are optically thick because the oil's extinction coefficient is on the order of 10^{+1}/mm throughout the region of interest. The water-dispersant mixture, however, has an extinction coefficient an order of magnitude smaller than that of the oil with scattering being the dominant mechanism. Diffuse radiation can possibly be transmitted through even relatively thick layers of water-dispersant mixture. For this reason, the boundary conditions assumed for the scattering method above do not strictly apply to the dispersant, and another method of determining the scattering coefficient had to be devised.

If it is assumed that there is no chemical reaction when the dispersant is mixed with water, then the individual atomic and molecular absorptions should not be altered significantly. This means that the absorption coefficient of the mixture will be the algebraic sum of the absorptions of the constituents weighted by their concentrations. Since the dispersant and water in their unmixed forms scattered such a small percentage of the specular beam that it could not be detected by our equipment, the scattering coefficient was assumed small enough so that the extinction coefficient could be taken equal to the absorption coefficient. Under these assumptions, the scattering coefficient will then be given by the difference between the algebraic sum described above and the extinction coefficient of the mixture presented in Section II.1. A simultaneous plot of these coefficients is given in Fig. 36.

The scattering coefficient for pure or natural waters is extremely small, and its evaluation requires substantial modification of the methods employed here. However, both natural and pure water have been frequently investigated, and the variations of optical parameters between different water types is small enough to justify using literature values for the present work (see Refs. [5, 6]).

II.3. INDEX OF REFRACTION

II.3.1. THEORY

The transfer of electromagnetic radiation from one material to another is governed by two sets of equations: Fresnel's Equations and Snell's Law. Because these equations are, at least implicitly, functions of the refractive index of the materials involved, many phenomena associated with this radiation transfer are potential sources of refractive index information. Of particular interest in connection with the present work are the formation of a critical angle and the specular reflectance at a dielectric boundary. These are discussed in this section in connection with the particular measurements in which they were employed. For more thorough treatments of these topics, see Refs. [7-9].

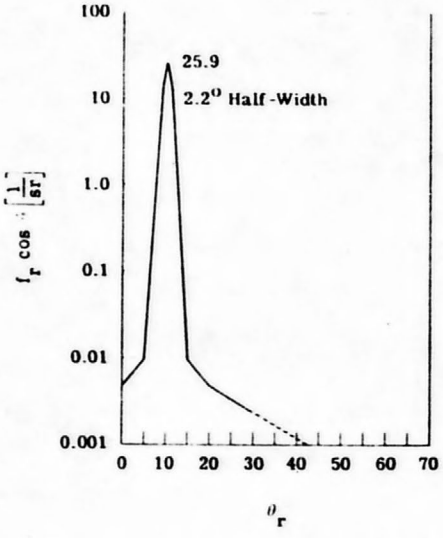

FIGURE 30. SANTA BARBARA OIL REFLECTION DISTRIBUTION FUNCTION. λ = 0.35-0.39 μm; θ_i = 10°; test mirror: f_r = 345, 2.1° half-width.

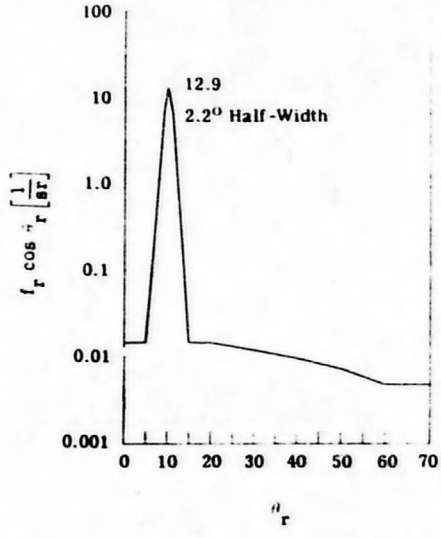

FIGURE 31. DISPERSANT-WATER MIXTURE REFLECTION DISTRIBUTION FUNCTION. λ = 0.35-0.39 μm; θ_i = 10°; test mirror: f_r = 345, 2.1° half-width.

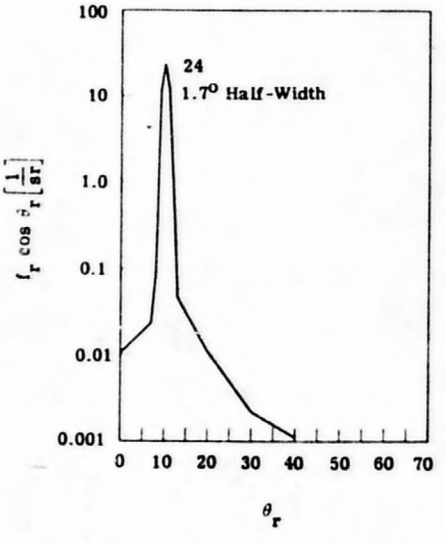

FIGURE 32. SANTA BARBARA OIL REFLECTION DISTRIBUTION FUNCTION. λ = 0.38-0.47 μm; θ_i = 10°; test mirror: f_r = 915, 1.6° half-width.

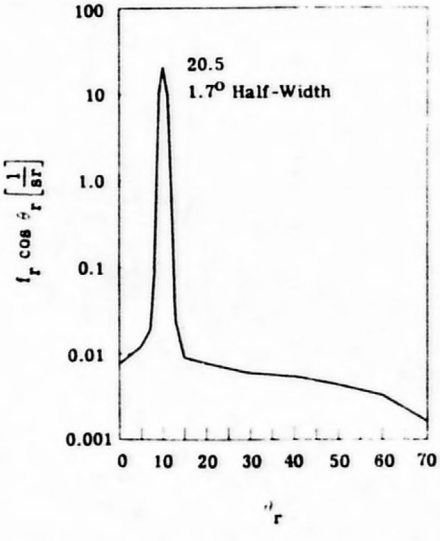

FIGURE 33. DISPERSANT-WATER MIXTURE REFLECTION DISTRIBUTION FUNCTION. λ = 0.38-0.47 μm; θ_i = 10°; test mirror: f_r = 915, 1.6° half-width.

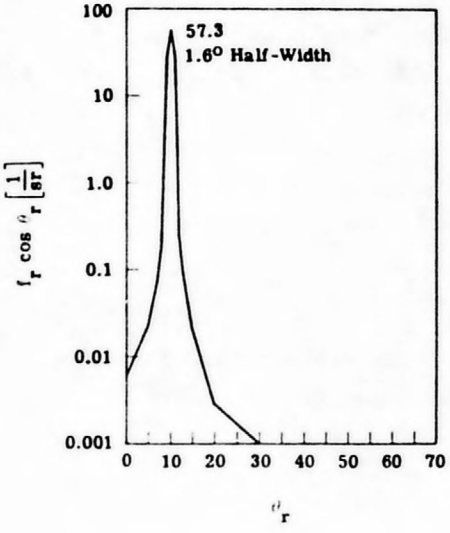

FIGURE 34. SANTA BARBARA OIL REFLECTION DISTRIBUTION FUNCTION. λ = 0.54-0.57 μm; θ_i = 10°; test mirror: f_r = 1240, 1.6° half-width.

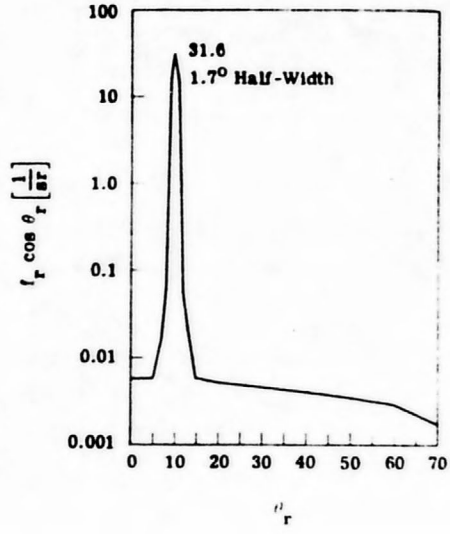

FIGURE 35. DISPERSANT-WATER MIXTURE REFLECTION DISTRIBUTION FUNCTION. λ 0.54-0.57 μm; θ_i = 10°; test mirror: f_r 1240, 1.6° half-width.

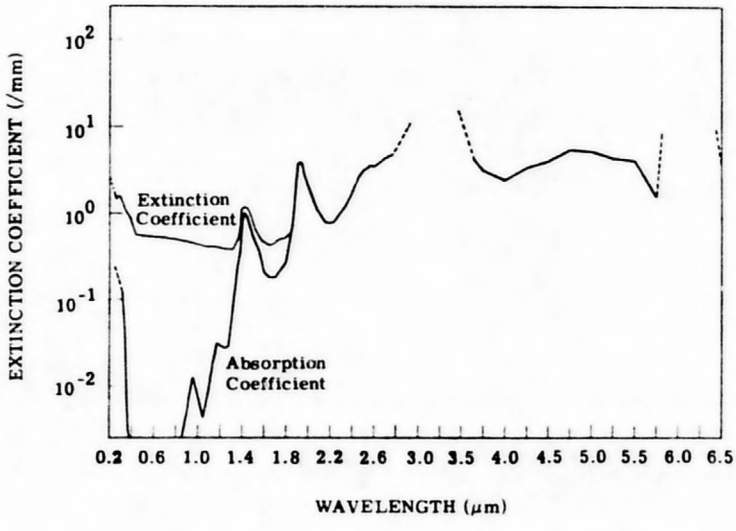

FIGURE 36. ABSORPTION AND EXTINCTION COEFFICIENTS — 40:1 MIXTURE OF SEA WATER AND DISPERSANT

The portion of an incident beam of light which is reflected as the beam attempts to cross a boundary between two materials is given by Fresnel's Equation:

$$\rho_{\perp} = \left| \frac{\sin(\theta_i - \theta_r)}{\sin(\theta_i + \theta_r)} \right|^2 \tag{28}$$

where $\rho_{\perp}$ = the reflection coefficient for light polarized perpendicular to the plane of incidence

θ_i = the angle off normal at which the light is incident on the boundary (angle of incidence)

θ_r = the angle off normal at which the light is transmitted into the second material (angle of refraction)

The relationship between the angle of incidence and the angle of refraction is given by Snell's Law:

$$n_i \sin \theta_i = n_r \sin \theta_r \tag{29}$$

where n_i = the index of refraction of the initial medium

n_r = the index of refraction of the final medium

If the incident medium is air, n_i may be taken equal to unity. Equation (29) may then be put in the form

$$\sin \theta_r = \frac{1}{n_r} \sin \theta_i$$

and therefore,

$$\cos \theta_r = \left(1 - \frac{\sin^2 \theta_i}{n_r^2} \right)^{1/2} \tag{30}$$

Substituting these expressions into Eq. (28) and solving for n_r, we obtain:

$$n_r = \left(\frac{\rho_{\perp}^{1/2} + 1}{\rho_{\perp}^{1/2} - 1} \cos^2 \theta_i + \sin^2 \theta_i \right)^{1/2} \tag{31}$$

Therefore, we have an explicit expression for the index of refraction of the final medium in terms of the incidence angle, θ_i, and the reflection coefficient of the material in air, $\rho_{\perp}$.

Since $\rho_{\perp}$ is defined as the ratio of reflected to incident radiation for radiation polarized perpendicular to the plane of incidence, we can write

$$\rho_{\perp} = I_{\perp} / I_{o\perp}$$

where $I_{\perp}$ = the intensity of reflected radiation

$I_{o\perp}$ = the intensity of incident radiation

If a reflectance measurement is then made of a material of refractive index n_1, we have from Eq. (28)

$$\left(\frac{I_{\perp}}{I_o}\right)^{1/2} = \frac{\sin \theta_{i1} \cos \theta_{r1} - \cos \theta_{i1} \sin \theta_{r1}}{\sin \theta_{i1} \cos \theta_{r1} + \cos \theta_{i1} \sin \theta_{r1}}$$

or substituting from Eq. (30) and simplifying

$$I_o = I_{\perp 1}\left[\frac{\sqrt{1 - \left(\frac{\sin \theta_{i1}}{n_1}\right)^2} + \cos \theta_{i1}\left(\frac{\sin \theta_{i1}}{n_1}\right)}{\sqrt{1 - \left(\frac{\sin \theta_{i1}}{n_1}\right)^2} - \cos \theta_{i1}\left(\frac{\sin \theta_{i1}}{n_1}\right)}\right]^2 \tag{32}$$

If it is assumed that the source of radiation remains constant between measurements, this value of I_o may be used in conjunction with the measured intensity from the sample to obtain ρ for the sample.

$$\rho_{\perp(\text{sample})} = I_{\perp(\text{sample})}/I_o$$

The only remaining parameter is θ_i which may be easily measured and is held constant for all intensity measurements. Experimental measurement of $I_{\perp}$ for each sample at each wavelength and Eq. (31) then determine the refractive index of the sample.

A second phenomenon associated with the transfer of radiation across a boundary is the formation of a critical angle. If we employ Snell's Law and require that the angle of refraction be 90°, we have

$$n_i \sin \theta_i = n_r$$

This then defines a "critical" incidence angle, θ_c:

$$\theta_c = \sin^{-1}\left(\frac{n_r}{n_i}\right) \tag{33}$$

and for incidence angles greater than this value the radiation is totally reflected back into the incident medium. However, it should be noted that this condition is possible only if $n_r < n_i$ since $\sin \theta_c$ cannot be greater than unity. The case $n_r = n_i$ is, of course, the trivial case where there is no interface and $\theta_r = \theta_i$.

Therefore, the refractive index n_r may be determined if the critical angle is measured at an interface between the sample and a material of known index (n_i).

$$n_r = n_i \sin \theta_c$$

In practice, a further consideration is necessary. Consider the case of a sample in contact with a parallel plate of higher refractive index as shown in Fig. 37. If the incident beam is introduced into the sample parallel to the interface 2, a critical angle, θ_c, will be formed in the second medium when $n_i > n_r$. The beam will then be incident on interface 1 between the second medium and air at an angle also equal to θ_c. However, a critical angle also exists for this interface and is given by

$$\sin \theta_c' = \frac{1}{n_i}$$

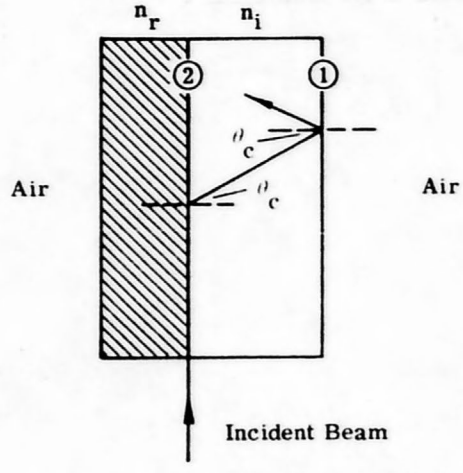

FIGURE 37. TWO-LAYER INTERFACE SHOWING CRITICAL ANGLE

and since

$$\sin \theta_c = \frac{n_r}{n_i}$$

we have that

$$\sin \theta_c' < \sin \theta_c$$

or, since θ is limited to values between zero and 90^o, we have

$$\theta_c' < \theta_c$$

and all the energy will be reflected back into the second medium and cannot be detected.

Therefore, in practice, it is necessary to incline interface 1 so that all rays are incident on it at angles less than θ_c'. This is done by making the higher index medium a prism with an apex angle, α, such that the above condition is satisfied. However, this complicates the measurement since the emerging beam will then be refracted upon leaving the prism, as shown in Fig. 38.

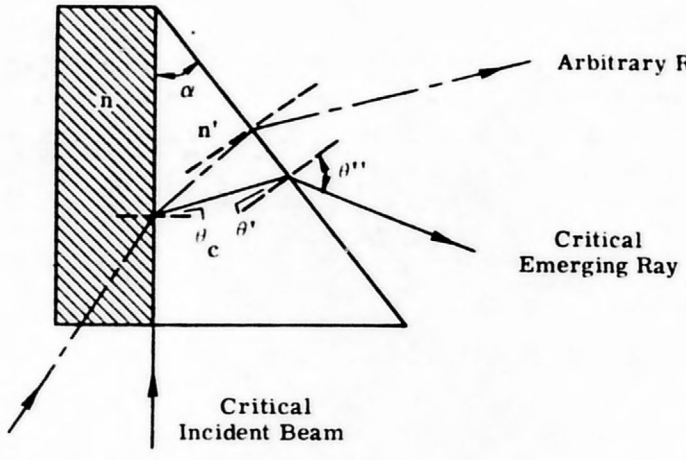

FIGURE 38. INCLINED INTERFACE SHOWING REFRACTION OF BEAM

By applying Snell's Law to each interface and noting that θ_c and θ' are related to the apex angle as

$$\theta_c + \theta' = \alpha$$

one has

$$n = n' \sin \theta_c$$

$$\sin \theta'' = n' \sin \theta'$$

Combining these equations in such a way as to eliminate θ_c and θ', one obtains

$$n' = \sin \alpha [(n')^2 - \sin^2 \theta'']^{1/2} \pm \cos \alpha \sin \theta'' \qquad (34)$$

where the (+) sign is used if the emerging beam is refracted toward the apex and the (-) sign is used if it is refracted away from the apex as in Fig. 38.

It should also be noted that any ray incident on the prism sample interface at an angle less than 90° will be refracted less than the critical ray. Therefore, diffuse light incident on the sample will result in a field of light being emitted from the prism. This field will end abruptly at the critical ray.

II.3.2. EXPERIMENTAL PROCEDURE AND RESULTS

Since the samples being tested had large absorption bands in the infrared and ultraviolet regions, the method used to evaluate the refractive index in these regions could not depend on transmission of radiation through the sample. The method employed in the present work was that of measuring the reflection coefficient of an air-sample interface. The experimental apparatus is shown in Fig. 39. For the absorption bands in the near ultraviolet and near infrared regions, the source was an air-cooled quartz-iodine lamp and the polarizer was a Glan-Thompson prism. For the infrared, a carbon glow-bar and Perkin-Elmer wire grid polarizer were used. The source was collimated by mirrors 2A and 2B polarized perpendicular to the plane of incidence and reflected off the sample. The reflected light was then gathered and focused on the entrance slit of the monochromator using mirrors 3A, 3B, and 3C. The beam, wavelength selected by the monochromator, was then detected, amplified, and measured.

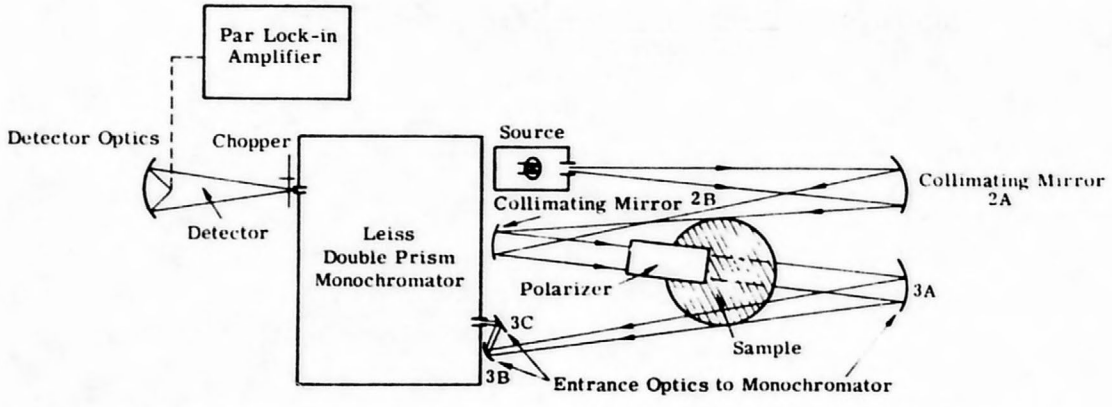

FIGURE 39. APPARATUS FOR MEASUREMENT OF REFLECTION COEFFICIENT

Because the reflection coefficient is the ratio of the reflected to incident intensities, a method was required for measuring the incident intensity. This is frequently accomplished by replacing the sample with a mirror and calculating the incident intensity from the reflection coefficient of the mirror. This method, however, necessarily limits the accuracy of all measurements to the accuracy with which this coefficient is known. The method used here, which circumvents this problem, was to replace the sample with distilled water whose refractive index is accurately known. Data collected in this way in conjunction with Eqs. (31) and (32) determines the refractive index of the sample.

In regions where absorption was not a problem, a more accurate method was used to determine the refractive index. This method depends upon the measurement of the critical angle formed at an interface between the sample and a material of higher refractive index. The apparatus is shown in Fig. 40. The source for the various wavelength regions was the same as those used in the reflection coefficient measurements discussed previously. The prism and

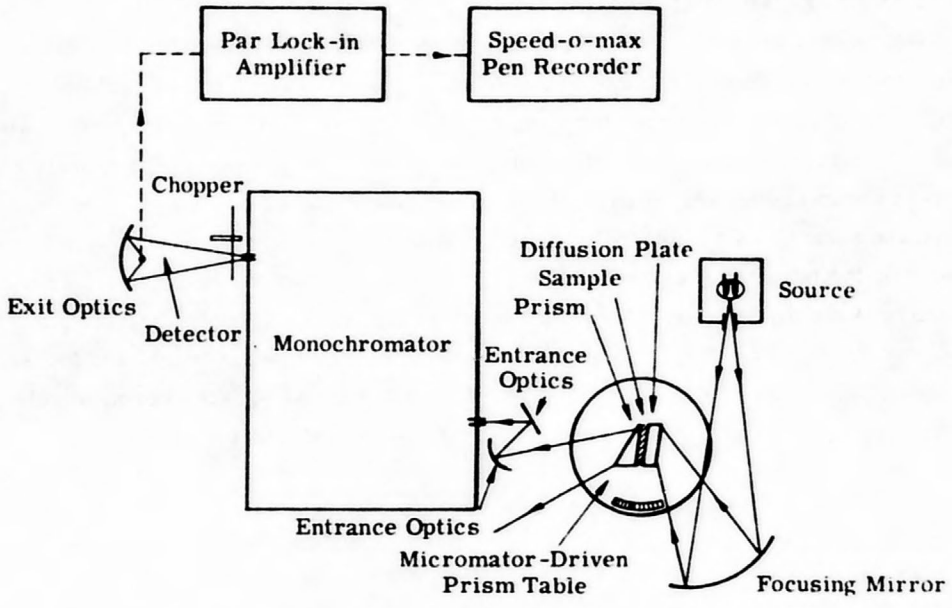

FIGURE 40. APPARATUS FOR MEASUREMENT OF CRITICAL ANGLE

diffusion plate were strontium titanate purchased for this application and cut and polished here at Willow Run Laboratories. Strontium titanate was chosen because it transmits well from 0.38 μm to 6.0 μm and has a refractive index in excess of 2.00 throughout this region. The detector was a photomultiplier in the visible and near-ultraviolet regions and was a lead sulfide cell in the near-infrared region.

Light from the source was focused on a ground strontium titanate parallel plate and, therefore, entered the sample at all possible angles. The emerging field of light was focused on the entrance slit of the monochromator in such a way that the demarcation line between light and dark, defined by the critical rays, was imaged on the entrance slit of the monochromator. The angle off normal to the prism face at which the critical rays were refracted was found by slowly rotating the prism table and locating the position of the table at which the energy was sharply cut off; in practice, this was done by finding the zero position of the table for which a ray normal to the prism face was imaged on the entrance slit, and then driving the table with a synchronous motor and plotting the energy "seen" by the detector. Since the refractive index of the prism is known, determination of these angles for each wavelength selected by the monochromator then determined the refractive index using Eq. (34).

Using both of these methods in the various spectral regions, we determined the refractive index of the oil sample, sea water, and a dispersant-water mixture. The results of these measurements are presented in Figs. 41 and 42.

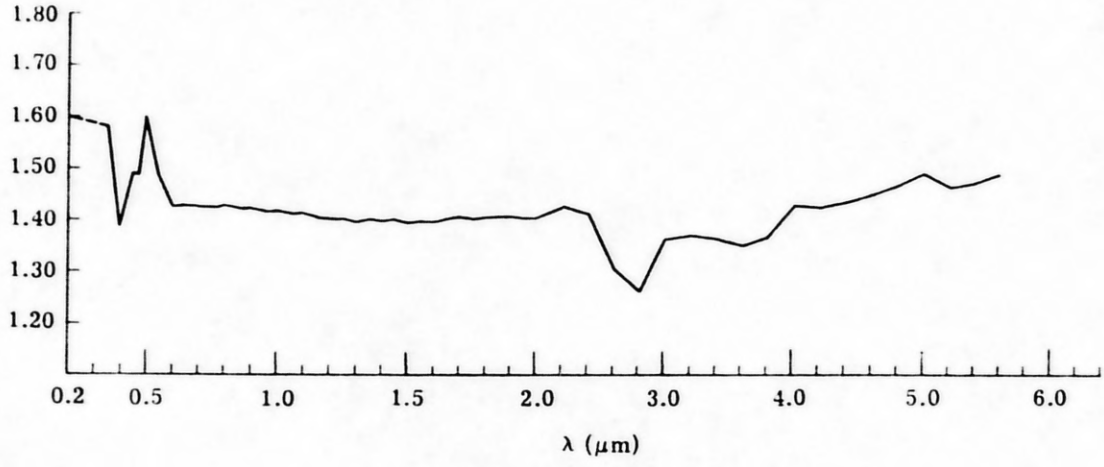

FIGURE 41. INDEX OF REFRACTION OF SANTA BARBARA OIL

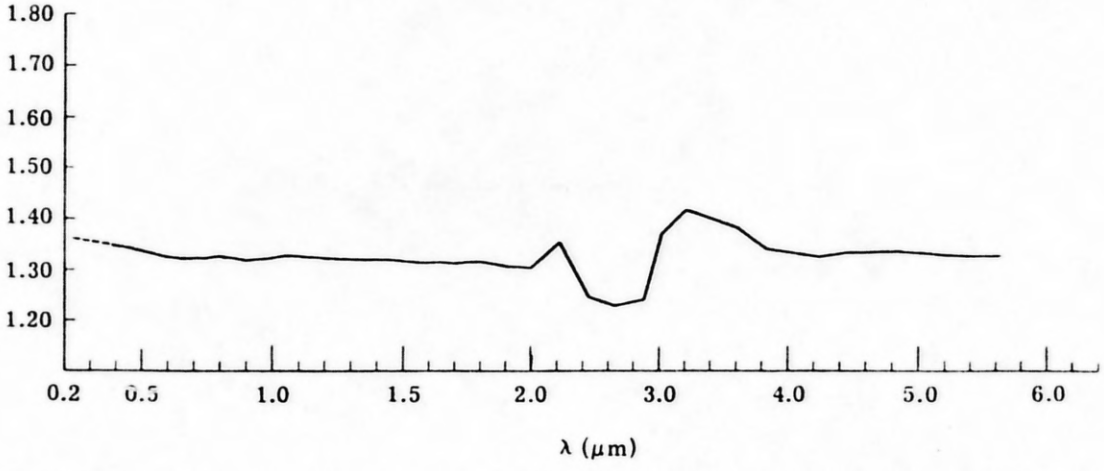

FIGURE 42. INDEX OF REFRACTION OF 40:1 MIXTURE OF SEA WATER AND DISPERSANT

Appendix III
DERIVATION OF THE DIFFUSE REFLECTANCE FOR TWO SEMI-INFINITE LAYERS OF AIR AND OIL

For semi-infinite oil and air layers meeting at an interface defined as x = 0, one has power flows and exitances as shown in Fig. 43.

The same general power flow equations apply as were used in the model for oil on the sea surface. The boundary conditions in the present case are:

at x 0 for specular power

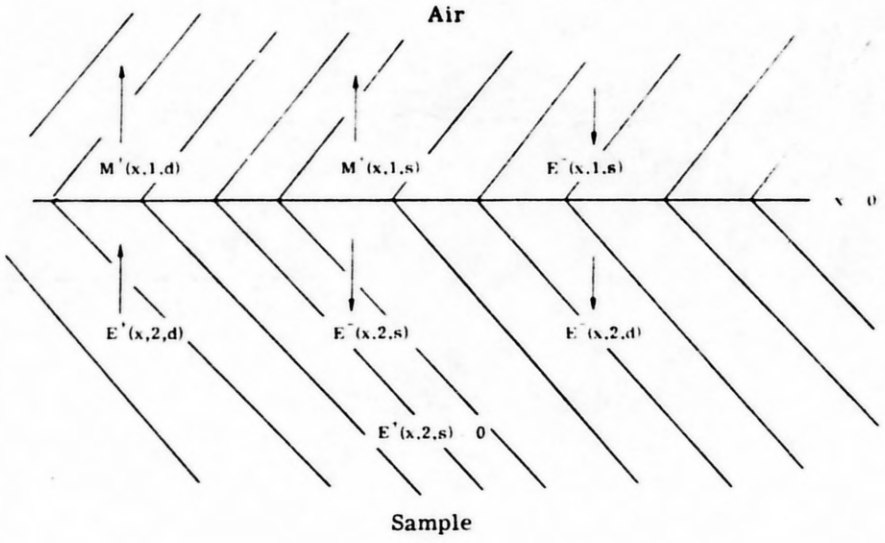

FIGURE 43. POWER FLOW AND EXITANCES FOR SEMI-INFINITE OIL AND AIR LAYERS

$$E^-(0,2,s) = [1 - \rho(1,2,s)]E^-(0,1,s)$$

$$M^+(0,1,s) = \rho(1,2,s)E^-(0,1,s)$$

at x = 0 for diffuse power

$$E^-(0,2,d) = \rho(2,1,d)E^+(0,2,d)$$

$$M^+(0,1,d) = [1 - \rho(2,1,d)]E^+(0,2,d)$$

at $x = -\infty$

$$E^{\pm}(-\infty,2,d) = E^{\pm}(-\infty,2,s) = 0$$

and

$$E^+(x,2,s) = 0$$

always since there is no reflection of specular power in the second layer.

The general solutions to the differential equations of flow still hold, as in Appendix I. Applying the boundary conditions, one eliminates certain coefficients and obtains expressions for the exitances and energy flows compatible with the problem at hand.

First of all, $E^{+}(x,2,s) = 0$, so that

$$0 = C_o e^{-\kappa_2 x}$$

and this implies

$$C_o = 0$$

But from the general solutions this gives

$$C = E = 0$$

We also have the condition that

$$E^{\pm}(-\infty,2,d) = 0$$

Therefore, symbolically

$$E^{+}(-\infty,2,d) = A(1 - b)e^{-g\infty} + B(1 - b)e^{+g\infty} + (F)e^{-\kappa\infty} = 0$$

$$E^{-}(-\infty,2,d) = A(1 + b)e^{-g\infty} + B(1 - b)e^{+g\infty} + (D)e^{-\kappa\infty} = 0$$

Therefore, this requires that either

$$g = \kappa = 0, \quad \text{and } A = B = F = 0$$

or that

$$B = 0, \quad g \neq 0, \quad \kappa \neq 0$$

Since the first of these alternatives is simply the trival case in which there is no oil present, the second choice must be true here. For the boundary condition at $x = 0$ for diffuse power flow,

$$E^{-}(0,1,d) = \rho(2,1,d)E^{+}(0,2,d)$$

or

$$A(1 + b) + D = \rho(2,1,d)[A(1 - b) + F]$$

and

$$M^{+}(0,1,d) = [1 - \rho(2,1,d)]E^{+}(0,2,d)$$

or

$$M^{+}(0,1,d) = [1 - \rho(2,1,d)][A(1 - b) + F]$$

The boundary conditions for specular flow at $x = 0$ give

$$E^{-}(0,2,s) = [1 - \rho(1,2,s)]E^{-}(0,1,s)$$

Therefore,

$$D_o = [1 - \rho(1,2,s)]E^-(0,1,s)$$

and

$$M^+(0,1,s) = \rho(1,2,s)E^-(0,1,s)$$

The second of these terms is recognized as simply the specular reflection from the interface. Recombining the preceding expressions, we get

$$A(1 + b) - 3f[1 - \rho(1,2,s)]E^-(0,1,s) = \rho(2,1,d)\{A(1 - b) - f[1 - \rho(1,2,s)]E^-(0,1,s)\} \quad (35)$$

$$M^+(0,1,d) = [1 - \rho(2,1,d)]\{[A(1 - b)] - f[1 - \rho(1,2,s)]E^-(0,1,s)\} \quad (36)$$

$$M^+(0,1,s) = \rho(1,2,s)E^-(0,1,s) \quad (37)$$

If it is assumed that we know the various optical parameters of the oil such as κ and n, the only unknowns are A and $M^+(0,1,d)$. The specular reflection coefficient of the system is then

$$\frac{M^+(0,1,s)}{E^-(0,1,s)} = \rho(1,2,s)$$

and the diffuse reflection coefficient is

$$\frac{M^+(0,1,d)}{E^-(0,1,s)} = [1 - \rho(2,1,d)]\frac{A(1 - b)}{E^-(0,1,s)} - f[1 - \rho(1,2,s)] \quad (38)$$

where A is still unknown. However, we also know from Eq. (35) that

$$A(1 + b) - \rho(2,1,d)(1 - b) = f\rho(2,1,d)[1 - \rho(1,2,s)]E^-(0,1,s) + 3f[1 - \rho(1,2,s)]E^-(0,1,s)$$

Therefore,

$$A = \frac{[1 - \rho(1,2,s)]fE^-(0,1,s)[3 - \rho(2,1,d)]}{(1 + b) - \rho(2,1,d)(1 - b)}$$

This then gives when substituted into Eq. (38)

$$\frac{M^+(0,1,d)}{E^-(0,1,s)} = [1 - \rho(2,1,d)]\left\{\frac{[1 - \rho(1,2,s)]f[3 - \rho(2,1,d)]}{(1 + b) - \rho(2,1,d)(1 - b)}(1 - b) - f[1 - \rho(1,2,s)]\right\}$$

or

$$\frac{M^+(0,1,d)}{E^-(0,1,s)} = f[1 - \rho(2,1,d)][1 - \rho(1,2,s)]\left\{\frac{[3 - \rho(2,1,d)](1 - b)}{(1 + b) - \rho(2,1,d)(1 - b)} - 1\right\}$$

If one now substitutes for the constant f using

$$f = \frac{\sigma}{8\sigma - 3k} = \frac{1}{2 - 3(\sigma/\alpha)}$$

and for b using

$$\frac{1+b}{1-b} = \frac{[1 + 2(\sigma/\alpha)]^{1/2} + 1}{[1 + 2(\sigma/\alpha)]^{1/2} - 1}$$

one obtains

$$\frac{M^{+}(0,1,d)}{E^{-}(0,1,s)} = \left[\frac{1}{2 - 3(\alpha/\sigma)}\right][1 - \rho(2,1,d)][1 - \rho(1,2,s)]\left\{\frac{[3 - \rho(2,1,d)]}{\frac{[1 + 2(\sigma/\alpha)]^{1/2} + 1}{[1 + 2(\sigma/\alpha)]^{1/2} - 1} - \rho(2,1,d)} - 1\right\}$$

and this is the expression for the diffuse reflection coefficient given in Section II.2.1.

REFERENCES

1. D. Hoult, Oil on the Sea, Plenum Press, New York, 1969.
2. P. G. Hasell and L. M. Larsen, Calibration of an Airborne Multispectral Optical Sensor, Report No. 6400-137-T, Willow Run Laboratories, Institute of Science and Technology, The University of Michigan, Ann Arbor, September 1968.
3. J. E. Estes and B. Golomb, "Monitoring Environmental Pollution," J. Remote Sensing, 2, Vol. 1, No. 2, March/April 1970, pp. 8-13.
4. R. Horvath, W. L. Morgan, and R. Spellicy, Measurement Program for Oil-Slick Characteristics, Report No. 2766-7-F, Willow Run Laboratories, Institute of Science and Technology, The University of Michigan, Ann Arbor, February 1970.
5. N. E. Dorsey, Properties of Ordinary Water-Substance, Reinhold Publishing Corp., New York, 1940.
6. E. O. Hulbert, "Optics of Distilled and Natural Water," J. Opt. Soc. Am., Vol. 35, No. 11, November 1945.
7. M. Born and E. Wolf, Principles of Optics, Pergamon Press, New York, 1959.
8. J. D. Jackson, Classical Electrodynamics, John Wiley and Sons, New York, 1952.
9. J. A. Stratton, Electromagnetic Theory, McGraw-Hill Book Co., New York, 1941.